



„POLITEHNICA" UNIVERSITY OF BUCHAREST

TRANSPORT DOCTORAL SCHOOL

PHD THESIS SUMMARY

RESEARCH ON WHEEL-RAIL SYSTEM VIBRATIONS

PhD Supervisor
Prof. dr. eng. Traian MAZILU

PhD Candidate
eng. Ioan Cristian CRUCEANU

DOCTORAL COMMITTEE

Chairman: Prof. dr. eng. Mihaela POPA
"POLITEHNICA" University of Bucharest

PhD Supervisor: Prof. dr. eng. Traian MAZILU
"POLITEHNICA" University of Bucharest

Members: 1. Prof. dr. eng. Ștefan SOROHAN
"POLITEHNICA" University of Bucharest
2. Prof. dr. eng. George STOICESCU
Technical University of Civil Engineering of Bucharest
3. Prof. dr. eng. Dinel POPA
University of Pitești

BUCHAREST

2021

Table of contents

Foreword **I**

List of tables **1**

List of figures

Lists of abbreviations and symbols **7**

1. Introduction **4**

1.1. The importance of studying the vibrations of the wheel-rail system 12

1.2. Scientific objectives of the thesis 15

1.3. Thesis overview 17

1.4. Published works 61

2. The current state of the research in the field of vibrations of the wheel-rail system 25

2.1. Railway modelling 26

2.2. Vehicle modelling 42

2.3. Wheel-rail interaction model 44

2.4. Research on structural analysis of beams on continuous elastic foundation 47

3. Railway modeling with nonlinear elastic characteristics **50**

3.1. Modelling of the nonlinear elastic characteristics of the rubber plates and the prism 52

3.2. Railway model 57

3.3 Movement of rail and sleepers under the action of static load 62

3.4. Linear model with homogeneous elastic characteristic 7

3.5. Equations of the dynamic response of the rail — linearized model with non-homogeneous elastic characteristics 10

3.6. Track dynamic response analysis 12

4. Modeling of the mounted axle **128**

4.1. Analytical method — Euler-Bernoulli beam theory with attached masses 128

4.2. Finite element method 19

5. Study of vibrations of the wheel-rail system **147**

5.1. Wheel-rail system modelling 148

5.2. Equations of the permanent harmonic mode 153

5.3. Equations of the random vibration mode 158

5.4. Vibration analysis of the wheel-rail system 163

6. Experimental tests for the validation of the theoretical model of the wheel-rail system 190

6.1. Measurement of accelerations and analysis of results 190

6.2. Validation of the theoretical model of the wheel-rail system 206
7. Thesis conclusions and personal contributions 217
7.1. Conclusions of the thesis 217
7.2. Personal contributions 49
7.3. Directions for research development 50
Bibliography 51

Introduction

Viewed from a historical perspective, railway transport has steadily evolved at the pace of the eras that have succeeded over almost two hundred years, but it has experienced a real revolution in the last 40 years when it became obvious the need to adapt to the requirements of a constantly changing society. Competing with road and air transport, rail transport has had to become faster, safer, more comfortable and, last but not least, more efficient and less polluting, in order to take its privileged place in the field of transport today.

One of these aspects is the vibration mode to which any railway vehicle is exposed during driving due to the phenomena of interaction between the vehicle and the superstructure of the roadway. Specific to railway vehicles is the fact that their vibrations are manifested over a very wide frequency range starting from 0.5 Hz and going up to 5000 Hz. Occupying such an extended frequency range, the vibrations of railway vehicles take different forms that can be highlighted by applying the principle of vibration decoupling, depending on the vehicle's own frequencies, as a mechanical system, or of some of its subsystems which become systems in their own right on the basis of that principle.

The study of wheel-rail vibrations is of particular practical importance in order to carefully identify the mechanisms by which these vibrations occur and to find the ways and means of diminishing them. Solving the problems raised by the vibrations of the wheel-rail system has attracted the attention of numerous researches over time, starting with Stephan Tymoshenko, who have systematically enriched scientific heritage through theoretical studies and experimental research. Through the proposed topic, the present work naturally fits into the general current of research in the field of vibrations of the redness system, contributing to the improvement of theoretical models of study of these types of vibrations. The improvements introduced in the model for the study of the vibrations of the wheel-rail system allow the investigation of new aspects of the vibrations of the wheel-rail system with the potential of applicability in order to improve the railway transport.

From a scientific point of view, the theme proposed in this thesis on the vibrations of the wheel-rail system falls within a much broader field with multiple applications, which is known by the generic name *of the mobile load problem* or *moving load problem* in the Anglosaxone literature [94]. In the dynamics of elastic structures, a mobile charge is meant a force that changes its support over time, and the aforementioned field has as its object of study the response of elastic structures to mobile loads.

In this work, a relatively simple solution is proposed, which, however, ensures a very good accuracy of the calculation, as will be seen along the way.

Thus, the first specific objective consists in approximating the elastic characteristics of the deformation force of the rail plates and the ballast prism by a bilinear function, characterized by an 'elastic' and a 'rigid' portion and a transition point from the elastic to the rigid portion. For this, for each individual case, the corresponding nonlinear resistance force was started from the nonlinear characteristic and the rigidity of the bilinear characteristic on the two portions and the coordinates of the transition point were determined. The scope of the bilinear characteristic and the errors that its use introduces in relation to the original nonlinear characteristic have also been determined. Achieving this goal required solving a complicated problem of minimum by the method of the smallest squares. The difficulty of the problem lies in the large number of variables to be taken into account and, because of this, the impossibility of solving it analytically.

The second specific objective was aimed at including these bilinear characteristics of the rail pads and the crushed stone porridge in the model of the rail considered as an infinite beam on the continuous foundation with two elastic layers. The first elastic layer introduces the effect of the rail pads, and the second elastic layer, the effect of the broken stone porridge. At this stage it is interesting to leave the rail under the action of static load (applied by the wheel). It is a nonlinear problem because by cumulating the two bilinear characteristics results in a characteristic with three branches of linear type and the length of the rail areas that support each portion must be calculated. In order to solve the equations obtained from the conditions at written limits for the junction sections of the different areas of the rail, an iterative procedure based on the Newton Raphson algorithm was developed.

Once the areas of the rail working on the different portions of the characteristic of the elastic foundation are delineated, one can move on to the third specific objective: the dynamic response of the rail, calculated in the form of a receptance. At this stage, the inertial effect of sleepers is also taken into account. Unlike the classic models in which the rail is represented by a beam on homogeneous elastic foundation (constant rigidity and damping along the foundation), in the present work, the elastic foundation is of the non-homogeneous type since the rigidity and damping change from one area of the rail to another corresponding to the three-branch characteristic.

The fourth specific objective results from the need to have a benchmark for comparing the results obtained with the new model. For this purpose, an equivalent model with homogeneous elastic characteristic was developed and the dynamic response of the rail was calculated. The equivalence parameters are the leaving of the rail and sleepers next to the static load.

The modelling of the mounted axle is the fifth specific objective. For this, a first analytical model is developed that is based on the theory of the Euler-Bernoulli beam with rigid bodies attached to shape the axle body and wheels. This model has the role of a reference for the second model, much more complex, which takes into account the complicated geometry of the wheels with the help of the method of finite elements. Similar results obtained with the two models in terms of their own low-frequency bending modes of the mounted axle give consistency to this approach.

The sixth specific objective is to assemble the model of the path and that of the mounted axle to finalize the model for the study of the vibrations of the wheel-rail system. The suspended mass of the bogie frame and the primary suspension are also taken into account, obtaining a comprehensive model with an extended frequency range.

After elaborating the model for the study of the vibrations of the wheel-rail system, the following two specific objectives are achieved: the comparison between the results obtained with the model proposed in this work, with a non-homogeneous foundation, and the results obtained with an equivalent classical model and, respectively, the analysis of the influence of the main nonlinear parameters of the rail plates and of the broken stone prism on the vibration level.

The last specific objective is to validate the proposed model by comparing the results obtained by measurements with those provided by applying the model with a non-homogeneous foundation.

The thesis structure is articulated into seven chapters as follows.

The first chapter highlights, as has already been seen, the importance of the theme addressed in this paper, the main objective, as well as the specific objectives. Finally, the papers

elaborated during the doctoral internship and published by the author under the coordination of the doctoral supervisor and the members of the guidance committee are reviewed.

The second chapter is dedicated to the analysis of the current state of research in the field of the theme, respectively the vibrations of the wheel-rail system.

Chapter 3 deals with the modeling with nonlinear characteristic. In the first subchapter, the procedure for approximating the nonlinear elastic characteristic of the rail plates and the broken stone prism by a bilinear function is presented. The model of the railway is then presented and the movement of the rail and sleepers under the action of static load is determined. The model equivalent to homogeneous elastic characteristic shall be drawn up on the basis of the movement of the rail and sleepers under the static load. The dynamic response equations are inferred for both the non-homogeneous elastic pattern and the equivalent model with homogeneous elastic characteristic. The last part is reserved for the analysis of the dynamic response, making a comparison between the results obtained with the two models.

In chapter 4 is presented the model of the mounted axle. In the first part, the analytical model of the mounted axle based on the Euler-Bernoulli beam theory with rigid masses attached is elaborated. As an illustrative element, it is considered the mounted axle of a passenger wagon currently in current operation on the CFR network. The symmetrical and antisymmetric excitation modes are highlighted and the frequency response functions, respectively the receptance in the wheel sections, are calculated and analyzed. In the second section of the chapter is presented the model of the mounted axle elaborated on the basis of the method of finished elements. It is a 3-D model consisting of almost 11000 tetrahedral elements with over 20000 knots. The ANSYS software package was used to run on the computer. The receptance of the wheels is calculated considering the two modes of excitation which is then compared with the wheel receptance obtained with the analytical model.

Chapter 5 deals with the study of the vibrations of the wheel-rail system with the help of previously elaborated models that are now integrated into the model of the entire system having as components the rail, the axle, the suspended mass of the bogie and the primary suspension. The relations of the elastic contact between the wheel and the rail are presented, starting from Hertz's nonlinear theory of contact between two elastic bodies. The equations of the permanent harmonic mode are inferred, calculating the expressions of the frequency response functions of the sizes of interest of the model: the displacement of the wheel and rail in the contact section with the wheel, the displacement of the suspended mass of the bogie, as well as the contact force and the force in the primary suspension. Next, the equations of the random mode are determined, and a procedure is presented for determining the extended spectrum of the wheel-rail excitation: the leveling of the path at low frequencies and the roughness of the treads at medium and high frequencies. The last part of the chapter is occupied with the analysis of wheel-rail vibrations, pointing out the relevant aspects that the model proposed in this work highlights.

Chapter 6 is intended to present the experimental tests carried out with the aim of having a referential in order to validate the theoretical model for the study of the vibrations of the wheel-rail system. The procedure for organizing the tests, the equipment used, is described in detail, and then the results obtained are analyzed. Specifically, the tests were carried out with an experimental train on current in-line traffic at different running speeds and had as their main objective the measurement of accelerations at the level of the axle box and the bogie frame from a passenger wagon. The analysis of the measured acceleration spectra showed the existence of wheel polygonalization defects, which allowed for the elaboration of a procedure for comparing the acceleration spectra measured with those determined by calculation, thus validating the theoretical model.

In the last chapter of the thesis, the 7th, are presented the main conclusions regarding the study of the vibrations of the wheel-rail system detached from the analysis of the theoretical results obtained. The original contributions are presented and a number of possible avenues for the development of further research are indicated.

The thesis ends with a bibliography chapter containing 172 bibliographic references.

Personal contributions

Chapter 3 aims to determine the dynamic response of the rail in terms of receptance by emphasizing the influence of the non-linearities of the elastic characteristic of the rubber wafers and the prism of the path. For this, an original model is developed that is briefly presented below.

Therefore, for the modeling of the path with nonlinear elastic characteristics, a model with two elastic floors is proposed, one for the rubber pads, and the other for the prism of the path, linearized around the equilibrium position of the path under the static charge. Characteristic of this model is the fact that the rigidity of the foundation changes along the path. Thus, there is an area around the static load where the foundation operates on the rigid portions of the elastic characteristics of the two elastic floors. Further, it is a transitional area in which the foundation works on the elastic portion of the rubber pads and on the rigid portion of the characteristic of the path prism, and then, at a greater distance from the static load section, the path foundation works on the elastic portions of the characteristics of the rail plates and the porch of the path. It is noted that the model is with non-homogeneous elastic characteristic, which is why further reference is made to *the linearized model with non-homogeneous elastic characteristic* (MLCEN).

For comparison, a linear pattern will be used, but with a homogeneous foundation, to which the elastic characteristic does not change along the path. It is obtained starting from the effect of the static load on the path, respectively the leaving of the rail and sleepers in the section where the static load acts. Basically, with the help of the path model with nonlinear elastic characteristic, the leaving of the rail and sleepers in the static load section is calculated, and then the elastic constants of a model with a foundation with homogeneous characteristic are determined. Reference should be made to this model as the *linear model with homogeneous elastic characteristic* (MLCEO).

Linear model with homogeneous elastic characteristic

Figure 22 shows the equivalent linear model consisting of an infinite beam of Euler-Bernoulli type, a characteristic homogeneous elastic.

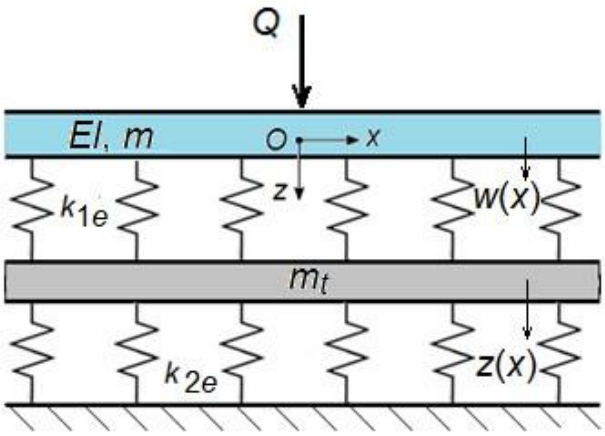


Fig. 22. Linear pattern with homogeneous elastic characteristic.

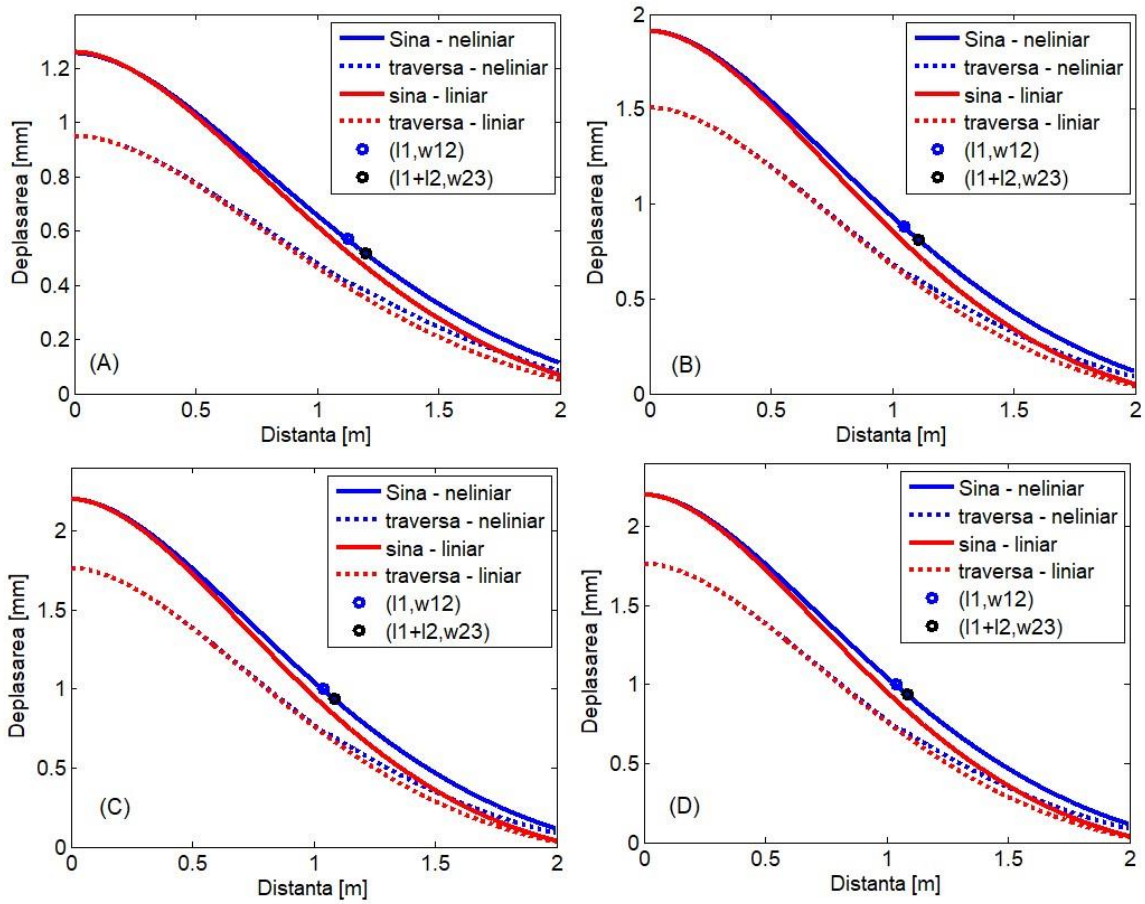


Fig. 23. Comparison between the nonlinear model and the MLCEO in terms of rail and sleeper movement.

Figure 23 shows the movement of the rail and sleepers along the path for the two types of models, considering the maximum values of the downforces, *Qo*. It is first of all noted that the displacement of the rail is greater than the displacement of the sleepers, which is justified by the effect of the elasticity of the rail plates. On the curve showing the displacement of the rail calculated according to the non-linear model are shown the transition sections from the rigid-rigid to the elastic rigid to the elastic-rigid characteristic and then from the elastic-rigid to the elastic-elastic characteristic. The results obtained with the two types of models are very close in the vicinity of the section where the static force acts, and then some differences appear. Thus, it is found that the movement of the rail and sleepers along the path are smaller in the case of the linear model with homogeneous elastic characteristic. Consequently, it shows that MLCEO overestimates the rigidity of the path.

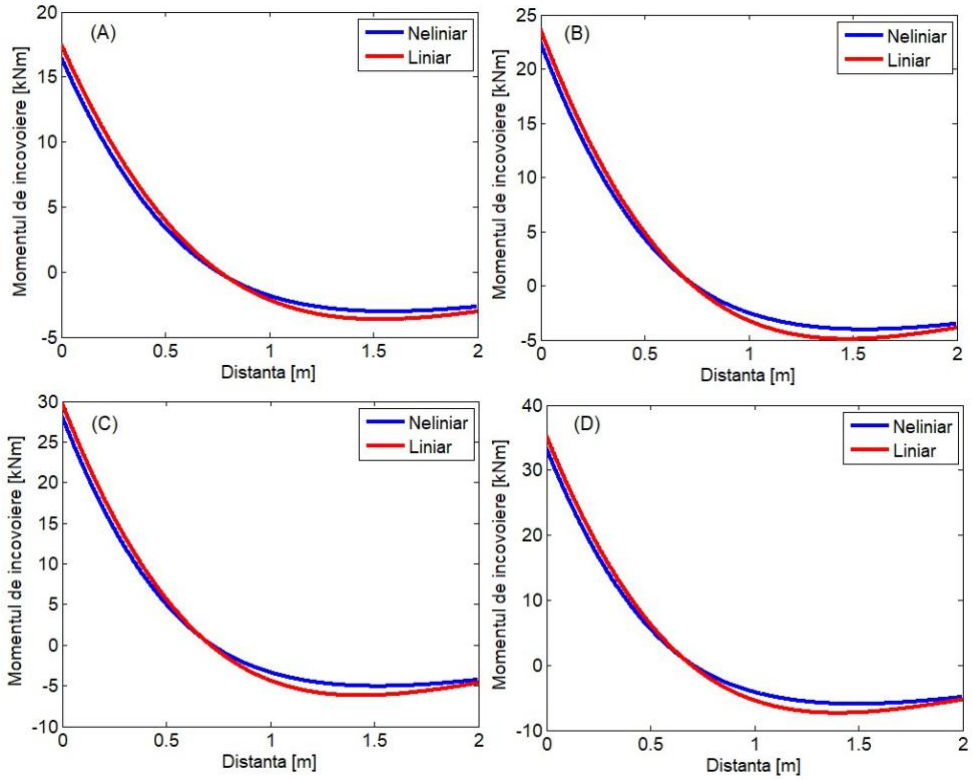


Fig. 24. Comparison between nonlinear model and MLCEO in terms of bending moment.

Figure 24 shows the bending moment along the path calculated with the two models. Obviously, the strain to which the rail is subjected due to the bending moment is maximum in the loading section and decreases as the distance increases from the load force section. Near the force, the MLCEO overestimates the value of the bending moment. Instead, the trend reverses in the field far from the load force.

The MLCEO will be used as a reference for reporting the results obtained using the nonlinear model for the permanent harmonic mode.

Linear model with non-homogeneous elastic characteristic

After calculating the movement of the rail and that of the sleepers under the action of the static load acting on the rail and the working portions of the elastic characteristics of the rubber plates and the prism of the path have been established, it is possible to proceed to the calculation of the dynamic response, respectively to the calculation of the receptance of the rail and the sleeper. This assumes that a ΔQ(t) harmonic force of ΔQ amplitude and ν frequency acts on the rail.

Basically, it is about linearizing the nonlinear model of the path around the equilibrium position below the static wheel load. Depending on the size of the static wheel load, three cases are distinguished as follows.

The first case concerns the situation where the static wheel load does not exceed the Q_{12} limit corresponding to the transition from the elastic to the rigid portion of the bililinear part of the path prism ($k_{22} \rightarrow k_{21}$). Both the rail pads and the prism of the path work on the elastic portions of the bilinear characteristics, and the resulting pattern has homogeneous elastic characteristic.

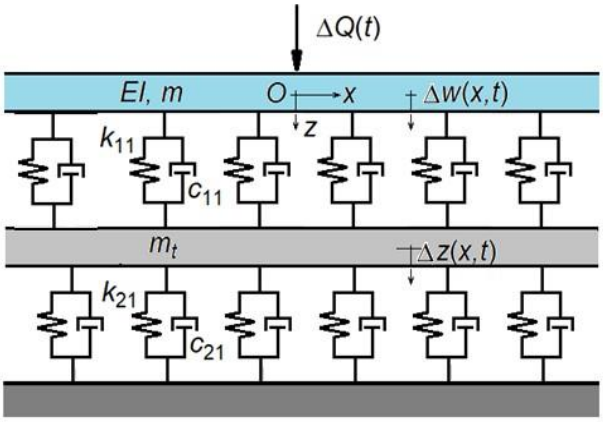


Fig. 25. The path model for the dynamic mode in the *elastic-elastic* case.

The second case occurs when the static wheel load exceeds the limit Q_{12}, but is less than the limit Q_{23}. The elastic wafers work only on the elastic portion of the bilinear characteristic, and the prism of the path works on the rigid portion of the bililinear characteristic in an area near the section of application of the static load. The length of this area is calculated as shown in § 3.3. For the rest, the prism of the path works on the elastic portion. The model is with non-homogeneous elastic feature.

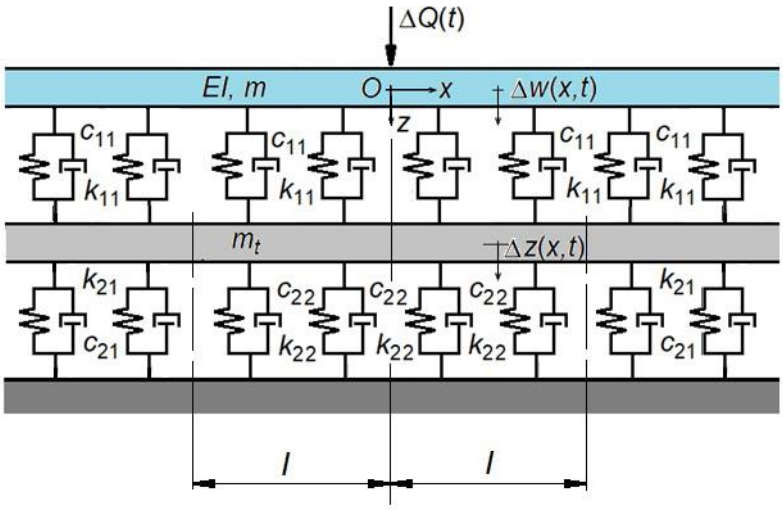


Fig. 26. The path model for the dynamic mode in the *case of elastic-rigid*.

If only the static load acts on the rail, then the transition from the rigid to the elastic portion of the characteristic of the path prism is delimited by a single section whose position is given by the calculation from § 3.3. When a dynamic (harmonic) force also acts on the rail, then, the elements of the inertial layer of the sleepers located in the immediate vicinity of the passage section will work, more or less, during compression, on the rigid portion, and during the relaxation on the elastic branch of the characteristic of the path prism. In other words, there is a transitional zone around the passing section along which the vibrational mode of the elements of the inertial layer of the sleepers is influenced by both the elastic and the rigid portion of the bilinear characteristic of the path prism. Now, if the amplitude of the dynamic force is small, then the influence of the vibration of the inertial layer of the sleepers in the area of transition from the rigid to the elastic portion of the characteristic of the ballast prism on the dynamic mode of the rail is negligible. As a result of this, the result is a linearized pattern with non-homogeneous elastic characteristic.

The last case occurs if the static wheel load is greater than the *limit* Q_{23}. This case is similar to the previous one with the difference that this time there are two transition sections, one when the transition from the rigid to the elastic portion of the biliniar portion of the rail plates ($k_{12} \rightarrow k_{11}$) is made, and the second, when the transition from the rigid to the elastic portion of the bilinial portion of the bilinear characteristic of the path prism ($k_{22} \rightarrow k_{21}$). The above considerations also apply in this case, resulting in a linearized pattern with non-homogeneous elastic characteristic.

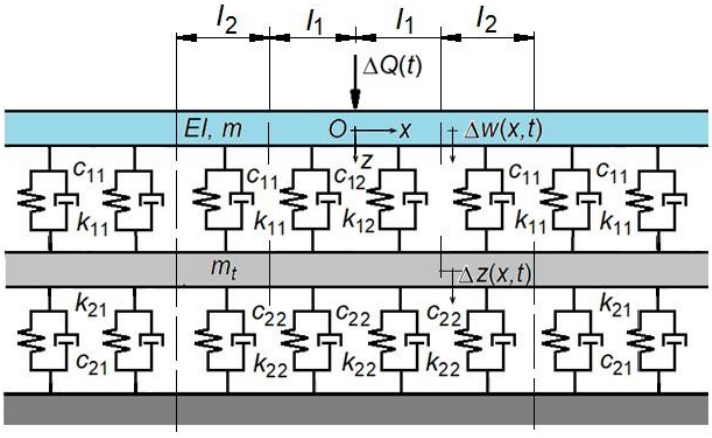


Fig. 27. The model of the path for the dynamic mode in the *case of rigid-rigid*.

Rigid-rigid case: Q > $_{Q23}$.

The *rigid-rigid* case is the general case and refers to the fact that both elastic structures end up working on their rigid portion in the central area around the section of the vertical load. To do this, the static load Q must exceed threshold load $_{Q23}$. Figure 27 shows the mechanical model reflecting this case.

Analysis of the dynamic response of the path

The following are the most important aspects of the dynamic response of the rail using MLCEN. As mentioned, as elements of comparison are taken the results that are obtained with the help of MLCEO.

Given that the maximum load up to which **the C** variant can be applied is 128 kN, which is greater than the static wheel load allowed on the European rail networks (125 kN), the parameters of the equivalent linear model corresponding to this variant are chosen for analysis.

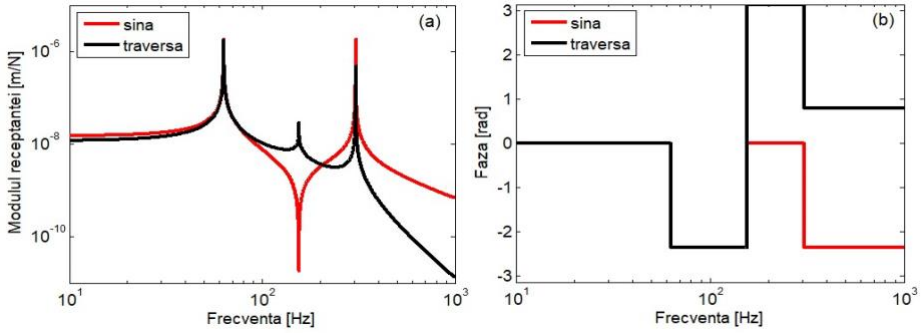


Fig. 28 The dynamic response of the rail and the crossbeam in the section of the harmonic force — MLCEO (case C): (a) the module of the receptance; (b) phase-shifting.

The MLCEO case without depreciation is initially considered. Fig. 28 shows the dynamic response of the rail and sleepers in the section of the harmonic excitation force, respectively the module of the receptance and the phase shift.

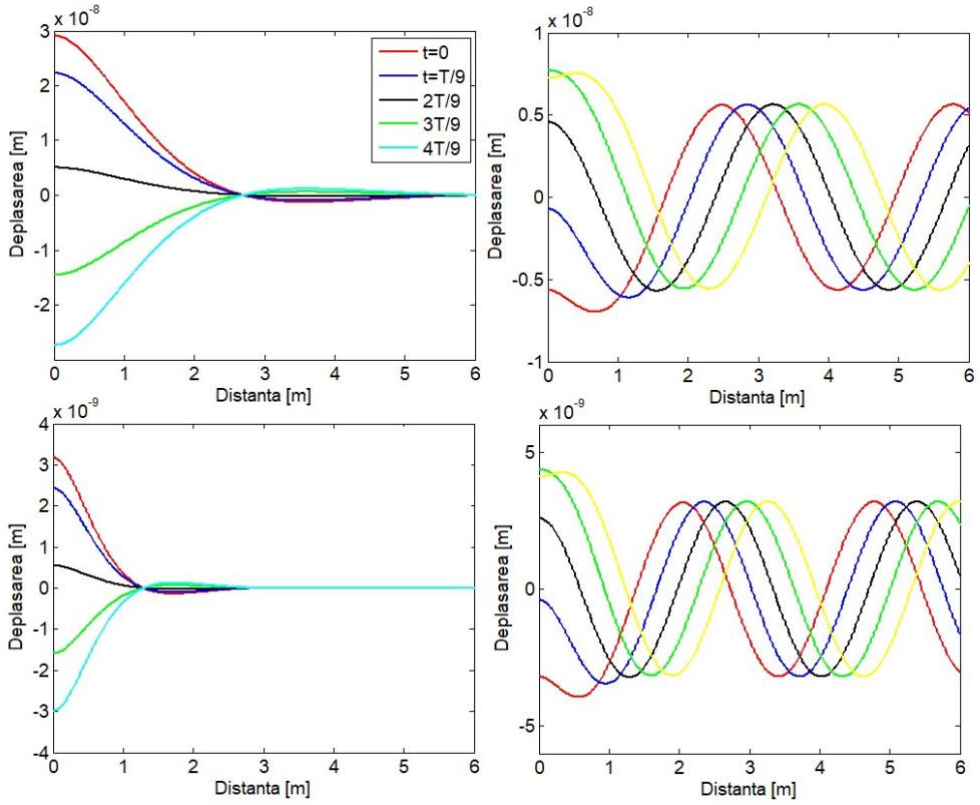


Fig. 29 Rail bending waves (MLCEO): (a) 50 Hz; (b) 100 Hz; (c) 200 Hz; (d) 400 Hz.

Comparing the results obtained with the two damping models, it is noticed that in the range of frequencies higher than the second resonant frequency they are similar: the calculated receptances tend asymptotically towards the receptances obtained with the model without damping. Also, both models influence the dynamic response of the path in the area of resonance and anti-resonance frequencies in the same manner, reduce the dynamic response next to the resonant frequencies and cause a certain amplification of it to the anti-resonance frequency. However, the dynamic response of the path at low frequency obviously has a lower amplitude in the case of hysteretic depreciation. Moreover, the receptance calculated with the hysteretic model does not tend to the perceived receptance with the unamortized model as it happens in the case of viscous depreciation, but is smaller than this, which signifies a stiffening of the path model.

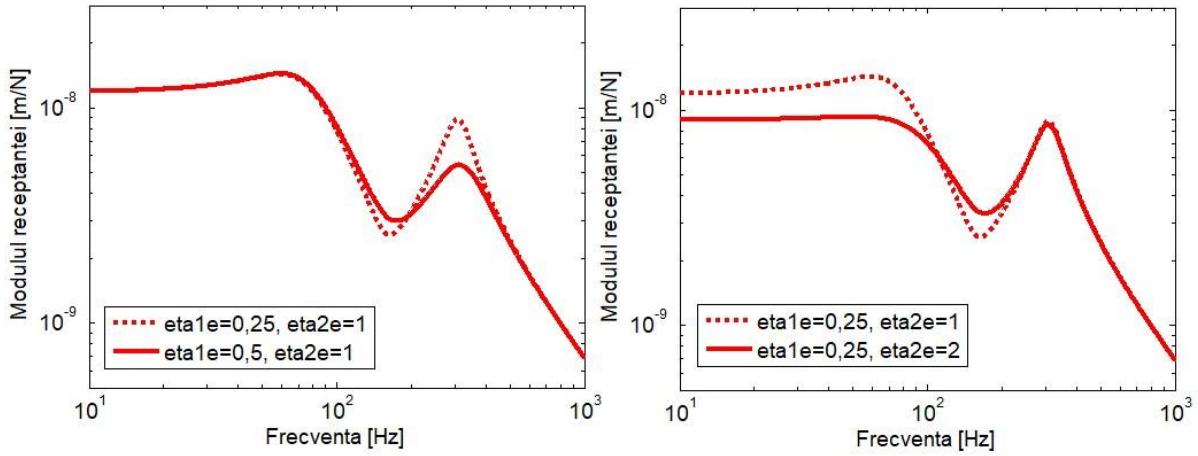


Fig. 34. The frequency ranges in which the hysteretic damping of rubber wafers and ballast prism influences the dynamic rail response (MLCEO).

Figure 34 shows the frequency ranges in which the hysteretic damping of the rail plates and the ballast prism influences the receptance of the rail. If, as regards the influence of the hysteretic depreciation of rubber wafers, the same tendency is observed as in the case of linear depreciation, then as regards the influence of hysteretic depreciation of the path prism, it is manifested not only by a reduction in the receptance in the area of the first resonant frequency and an increase in the receptance of the rail to the anti-resonance frequency, but also by a stiffening over the entire range of frequencies below the first resonant frequency.

A very important aspect of the dynamic response of the rail that influences its ability to produce noise is related to how it decreases the amplitude of the bending waves along the path. If the amplitude decreases less in relation to the distance to the excitation point, then the vibration of the rail is more intense and, as a result, the amount of mechanical energy converted into acoustic energy is greater – the noise produced by the rail is more intense.

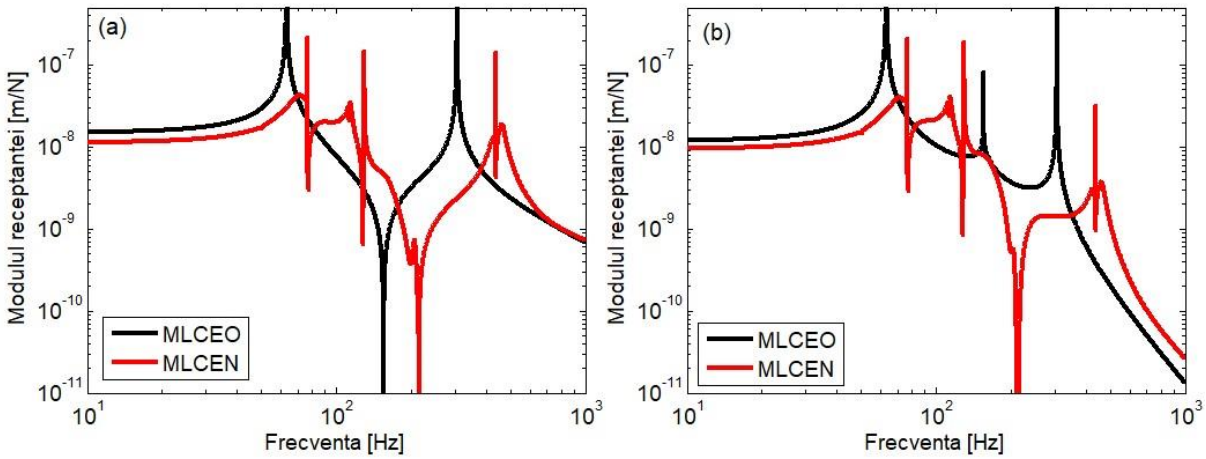


Fig. 38. Dynamic track response – quantitative comparison MLCEN - MLCEO (case C): (a) track receptance; (b) the receptance of sleepers.

Figure 38 allows for a quantitative comparison of the results obtained with the two track-side models. It is noted that the track receptacles and that of the sleepers calculated with MLCEN have a series of peaks at the following frequencies: 76,6, 113,8, 129,9 and 436,8 Hz. At the same time, anti-resonance modes can be observed both for the rail and for sleepers at

77,2, 128,3, 211,3 and 437,7 Hz. It is recalled that the MLCEO has two resonance frequencies at 63,3 Hz and at 306,0 Hz, as well as an anti-resonance frequency at 155,2 Hz. None of these MLCEO values are found among the homologous values given by the MLCEN calculation. In addition, at low frequencies, the receptacles resulting from MLCEO application are higher than those from MLCEN, which indicates that MLCEO underestimates the rigidity of the path.

Given that such large differences arise between the results obtained with the nonlinear model and the equivalent linear model, further investigation is needed to find the reason for these differences.

The causes of these differences lie in the MLCEO rigidity values which are much different from those of the rigid-rigid zone surrounding the excitation force in the MLCEN case and which determine the main characteristics of the rail receptance diagram in the section of the excitation force.

A better fit may be indicated if rigid-rigid-rigid MLCEO is taken into account instead of the equivalent MLCEO. However, there are important differences in the frequency range between the first resonant frequency and the anti-resonance frequency. First there is a discrepancy between the results given by the two models in the area of the first resonant frequency. Secondly, the MLCEN shows the existence of an area where the behaviour is of an anti-resonance type at 150 Hz followed by a zone dominated by a peak of the receptance at 162 Hz. These differences can be explained by the fact that in the case of MLCEN, in this frequency range, it propagates in the area around the excitation force (rigid-rigid) stationary propagation waves characterized by the existence of ventrs and nodes. These waves are the result of overlapping the direct waves departing from the section of the excitation force and the waves reflected by the inhomogeneity of the elastic foundation in the section where the rigid-rigid to the elastic-rigid area is passed from the elastic-rigid area and then after a very small distance to the elastic-elastic zone. In contrast, in MLCEO, due to the homogeneity of the elastic characteristic of the foundation, these type of waves (stationary propagation) does not occur.

The calculations were performed for 6 relevant frequencies to cover the frequency ranges in which the dynamic response of the rail shows the peculiarities that were revealed above. The charts show important differences at all calculation frequencies between how each model assesses bending wave attenuation along the rail, regardless of the damping pattern used. The biggest differences are between the results given by the MLCEN and the MLCEO equivalent.

Chapter 4 presents the model of the axle mounted for further use for simulating the vibrations of the wheel-rail system. As a numerical application, the axle of a 19-55 series passenger car that can run at speeds of up to 140 km/h on the Romanian rail network (CFR) was considered as a numerical application. The wagon is equipped with Minden-Deutz bogies that are equipped with brake blocks.

Two methods are used to calculate the dynamic response of the axle mounted next to the wheels, namely, an analytical method based on the Euler-Bernoulli beam theory and the finished element method. The rationale for doing so starts from the fact that the finite element method is a very powerful theoretical instrument of high precision over a large frequency range, but there are situations in which this method can give erroneous results due to sensitivity, especially in the case of complicated structures, such as the railway wheel. In such an eventuality it is recommended that the results obtained with the finished element method be validated either experimentally or by means of a simple analytical model that gives reliable results but in a limited frequency range, usually at low frequency.

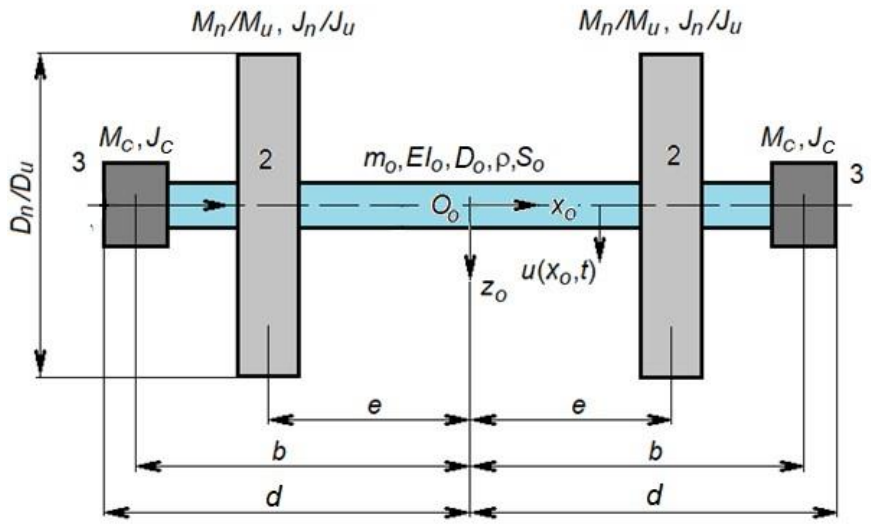


Fig. 1. Mechanical model 2 - D for the analytical method: 1) axle; 2) wheels; 3) axle boxes.

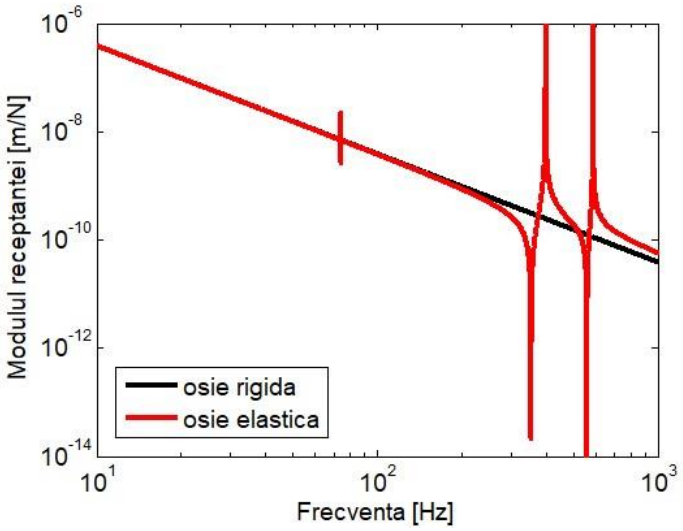


Fig. 3. Wheel receptance at symmetrical excitation at the tread.

Figure 3 shows the wheel-level acceptance for the case of symmetrical excitation applied to the treads being considered as the wheels in the new state; the frequency range is between 10 and 1000 Hz.

The receptance of the wheel has a bivalent character. On the one hand, the wheel receptance has an inertial character, its graph overlapping that of the receptance of the rigid axle over a wide frequency range. It should be noted that this characteristic of the wheel receptance is manifested at low frequencies and up to near the second resonant frequency when the wheel receptance begins to deviate sensibly from the purely inertial character.

On the other hand, the wheel receptance has a resonant-anti-resonant character. The calculations show that in the frequency range considered, the mounted axle has resonances at 74.35 Hz, 399.1 Hz and 589.7 Hz. Anti-resonance character manifests itself at frequencies lower than the resonant frequencies and is explained by the fact that the axle is crossed by

propagation bending waves that are emerging from the sections where the excitation forces act (in this case, from the sections of the wheels) and propagates to the two ends of the axle where their reflection takes place. The reflected waves overlap the direct waves and thus the stationary waves are formed.

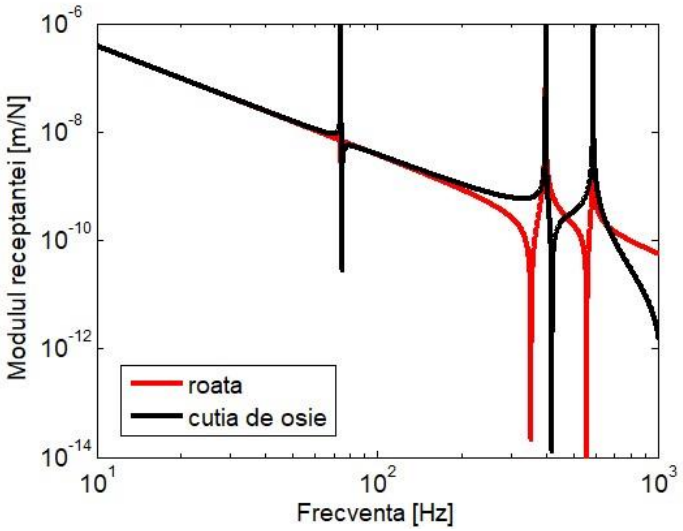


Fig. 4. Receptance of the wheel and axle at the axle box at symmetrical excitation at the tread.

Figure 4 shows the front of the wheel and the axle box when the mounted axle is symmetrically aroused at the level of the running surfaces. Obviously, the resonance frequencies of the mounted axle are not changed because they are an intrinsic property, but the anti-resonance frequencies change depending on the section of the axle that is being taken into account. At the axle box level, anti-resonance frequencies occur at frequencies higher than resonant frequencies.

Figure 5 shows the graphs of the receptances next to the wheel and next to the axle box when the mounted axle is symmetrically excited at the level of the axle boxes. As has been shown, this type of excitation helps to take into account the forces acting on the axle mounted by means of the primary suspension. The wheel receptance shows the anti-resonance mode at frequencies higher than the resonant frequency, respectively at 74,95 Hz and at 420,7 Hz. Anti-resonance after the third resonant frequency at 589,7 Hz occurs at a frequency greater than 1000 Hz as the calculation limit is considered.

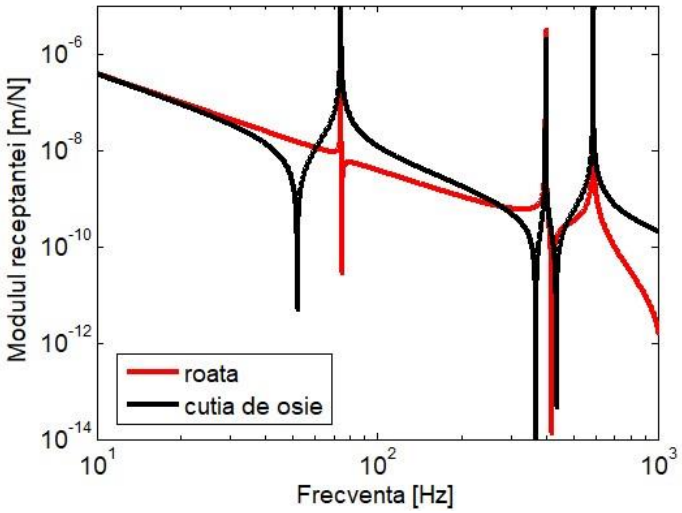


Fig. 5. Receptance of the wheel and axle at the axle box at symmetrical excitation at the level of the axle boxes.

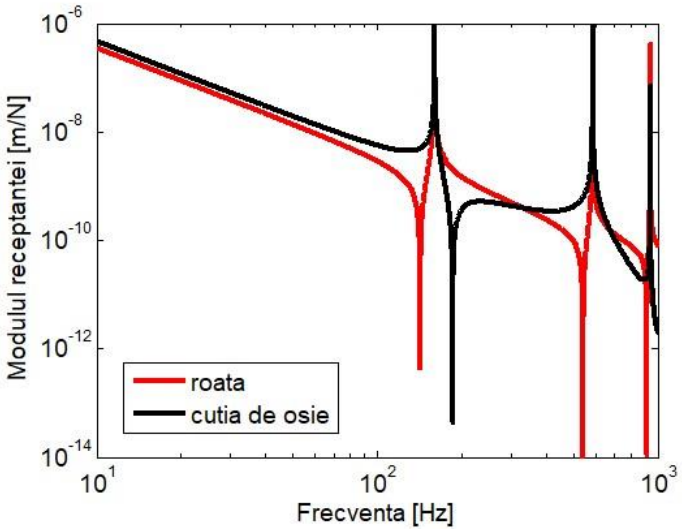


Fig. 6. Receptance of the wheel and axle at the axle box at antisymmetric excitation at the tread.

Receptance at the axle box level experiences the anti-resonance mode at frequencies significantly lower than the resonance frequency. Thus the first anti-resonance of the axle box occurs at 52 Hz, the second at 368.3 Hz, and the third anti-resonance frequency can be observed at 435.8 Hz.

Although the model developed in Chapter 5 regarding the vibrations of the wheel-rail system is based on the hypothesis of the symmetry of the vehicle and, from this point of view, is of interest only to symmetrical modes of excitation, in order to show the possibilities of the analytical model, the results obtained for the antisymmetric excitation modes are briefly presented.

Figures 6 and 7 show the dynamic response of the axle mounted at wheel and axle box level when the excitation is antisymmetric. In Figure 6, the antisymmetric excitation is at the level of the treads, while in Figure 7, it is applied at the level of the axle boxes.

Due to antisymmetric excitation, the dynamic response of the mounted axle is given by its own antisymmetric modes. In the frequency range under analysis, the resonance frequencies of the antisymmetric modes of the wheelset are at 160.5 Hz, 587.8 Hz, and 942.0 Hz

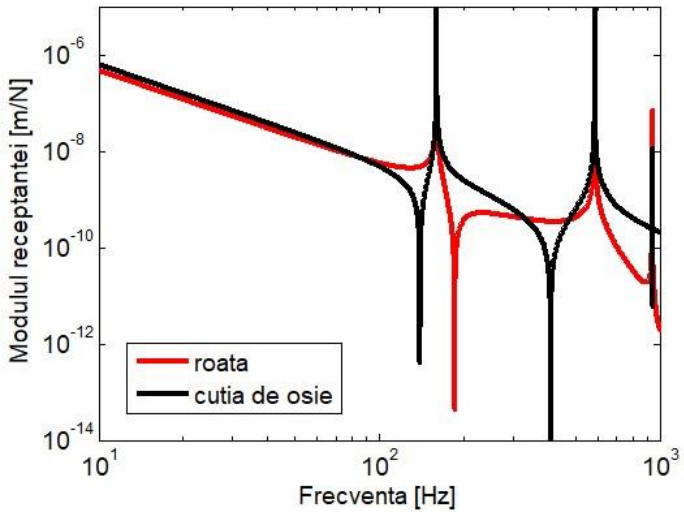


Fig. 7. The receptance of the wheel and axle at the axle box at antisymmetric excitation at the level of the axle boxes.

It is interesting to note that at low frequency, in the field where the inertial character of the dynamic response of the mounted axle is manifested, the receptance to the axle box is higher than that at the level of the wheel regardless of whether the antisymmetric excitation is applied to the wheel tread or to the level of the axle boxes. The explanation lies in the fact that the distance between the axle boxes is greater than the distance between the wheels and thus, at the same angle of inclination of the axle mounted as a result of the application of the antisymmetric force system, the displacement of the axle box is greater than the displacement of the wheel.

As for the anti-resonant mode, it manifests itself in a manner similar to the case of symmetrical excitation in the sense that if the antisymmetric excitation is on the wheels, then the anti-resonance frequencies of the wheel receptance are lower than the resonance frequencies, and the anti-resonance frequencies of the axle box are higher than the resonant ones (as in the case of symmetrical excitation). If the antisymmetric excitation is at the level of the axle boxes things happen the other way around, the receptance of the wheel has the anti-resonance frequencies higher than the resonance frequencies, and the receptance of the axle box has the anti-resonances at frequencies lower than the resonant frequencies.

Finite element method

In this section is presented the modelling of the axle mounted using the finished element method [19]. To do this, the ANSYS program package with the harmonic response module is used.

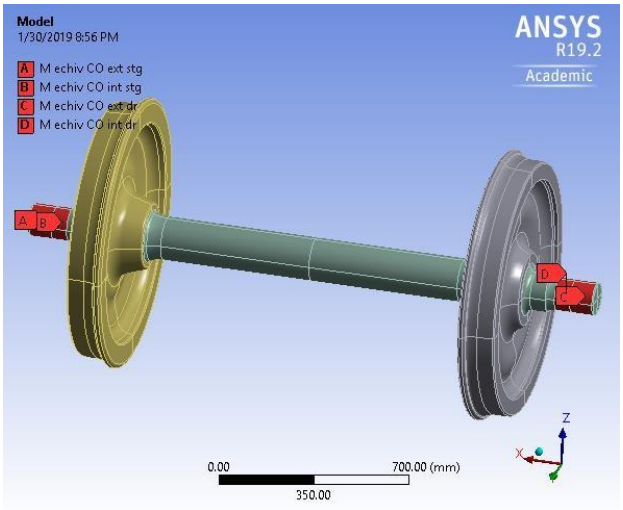


Fig. 8. Mechanical model 3 - D for the finite element method.

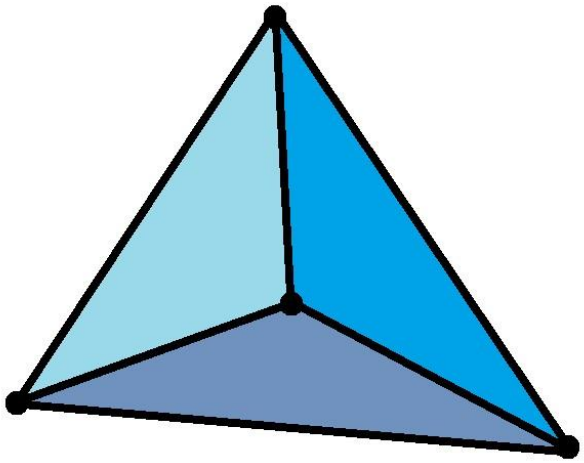


Fig. 9. Tetrahedral element used for bone discretization.

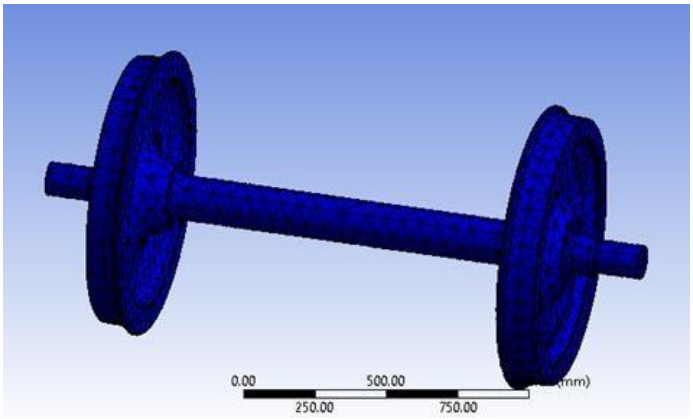


Fig. 10. The scheme of discretization of the axle.

Figure 8 shows the 3-D model of the Minden-Deutz bogie axle from a 19-55 series passenger wagon that was used for the numerical application of the analytical method (v. § 4.1).

For modeling with finished elements, tetrahedral elements (fig. 9) with an average size of 70 mm were used. The diagram of discretization with tetrahedral elements of the mounted axle comprises 10978 elements with 20110 knots and is shown in Figure 10.

The creation of the 3D model and simulation of the harmonic response in the ANSYS work environment was based on references [98] and [117].

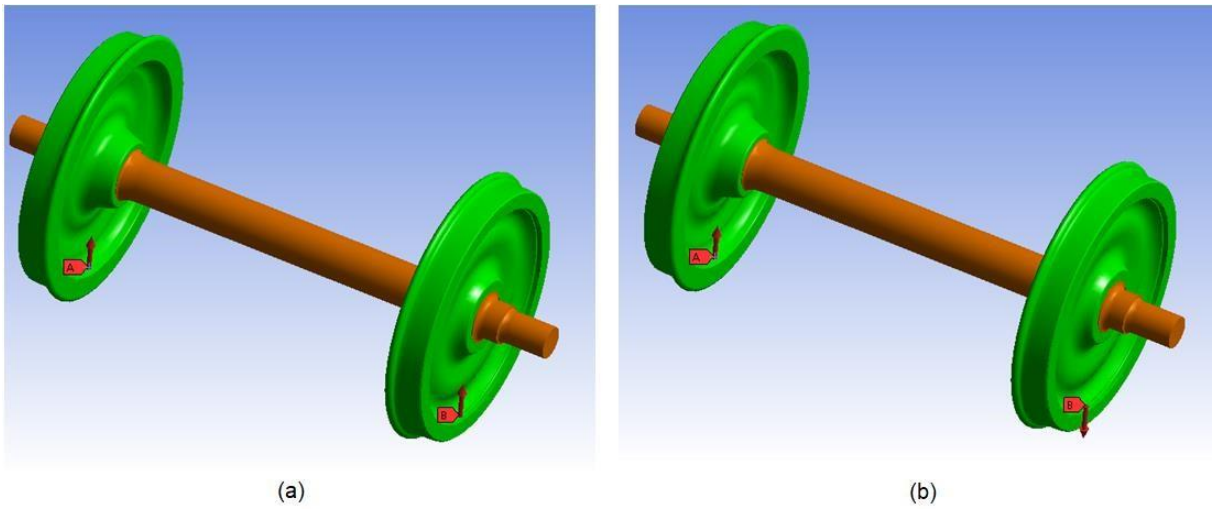


Fig. 11. Axle excitation on treads: (a) symmetrical; (b) antisymmetric.

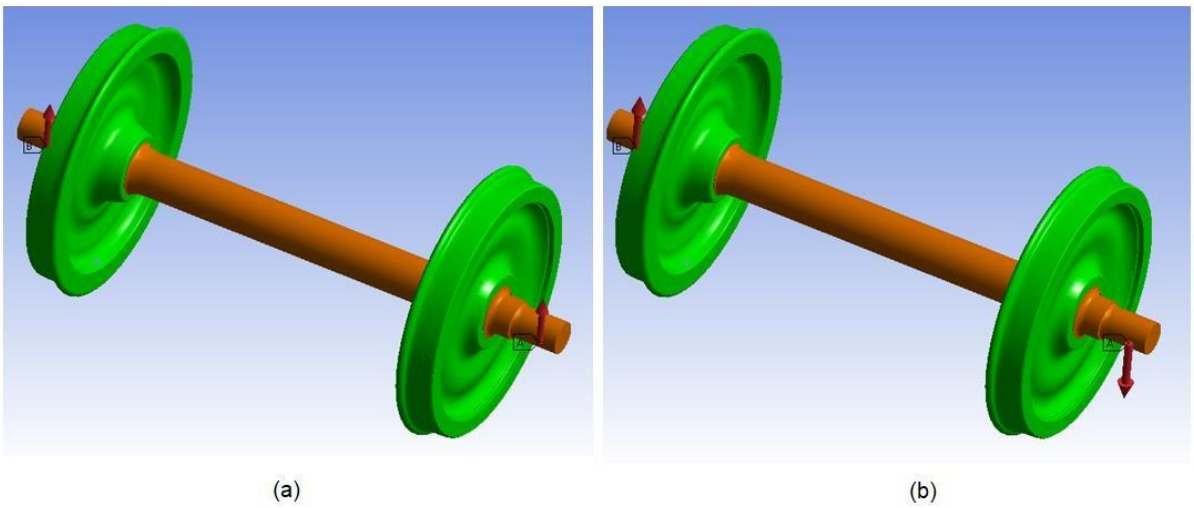


Fig. 12. Axle excitation in axle boxes: (a) symmetrical; (b) antisymmetric.

For the calculation of the dynamic response, 50 own modes were considered that cover the frequency range stretching up to 1000 Hz. Harmonic forces with an amplitude of 1N were applied to the running surface of the wheels, considering two situations of excitation, symmetrical excitation – the two forces are in phase (fig. 11 a), and antisymmetric excitation when the two excitation forces are in antiphase (fig. 11 b). It was also calculated the frequency response at the level of the axle wheels and boxes if harmonic forces with an amplitude of 1 N are acting on the axle (Fig. 12).

The vibration of the mounted axle is the result of the overlap of the 50 own modes considered. It should be noted that, in general, an own way of vibration of an elastic system,

such as the mounted axle, is related to the mode of unamortized free oscillations that occur at a certain frequency of its own in the form of a harmonic vibration and present a certain distribution of amplitudes. If the system is excited by a periodic disruptive factor whose frequency is equal to the frequency of a certain own way of vibration, then the elastic system shows the phenomenon of resonance.

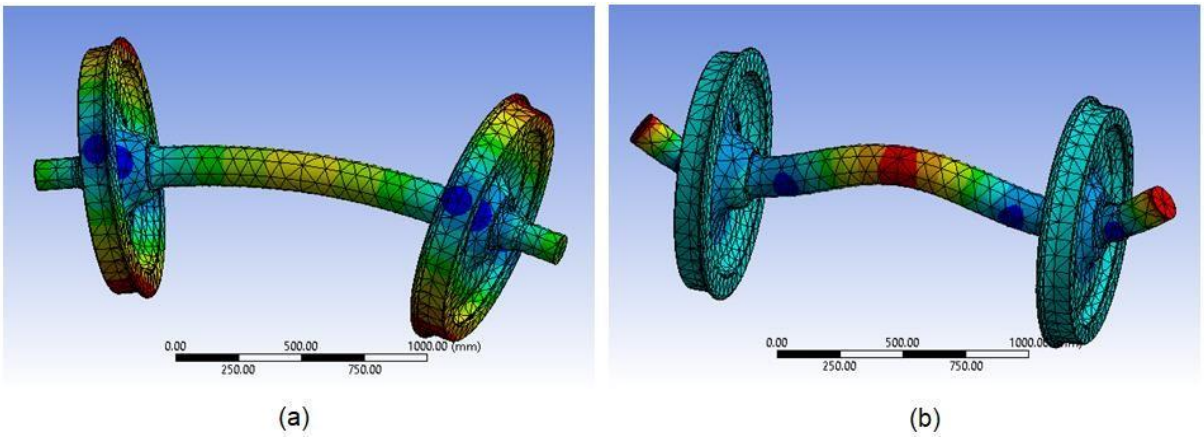


Fig. 13. Symmetrical bending modes: (a) the first mode; (b) the second mode.

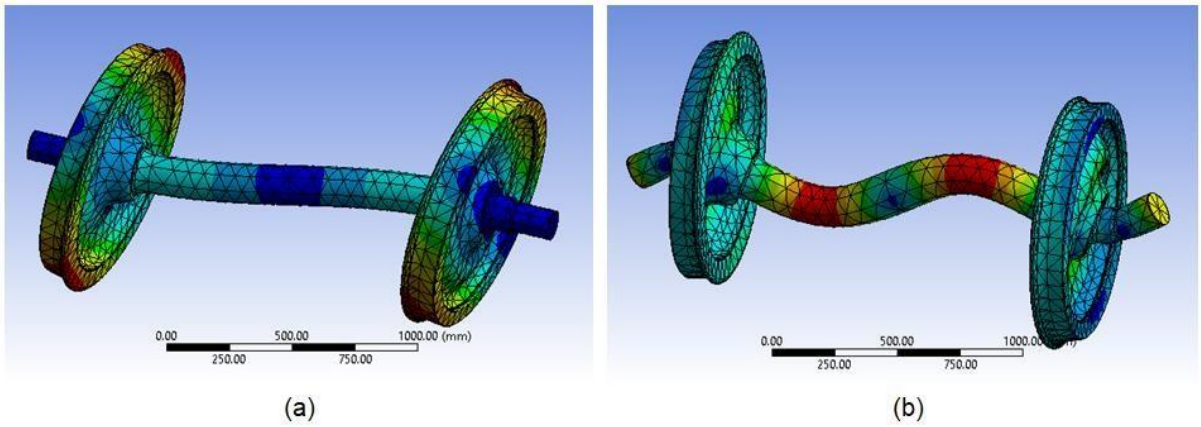


Fig. 14. Antisymmetric bending modes: (a) the first mode; (b) the second mode.

For the vertical response of the mounted axle, the most important are the own bending modes. They are symmetrical and antisymmetric according to whether the excitation is symmetrical or antisymmetric. Figures 13 and 14 show the first two own bending modes of the mounted axle, namely symmetrical and antisymmetric. The characteristic form of the distribution of amplitudes along the axle according to the type of its own mode is observed. In the case of its own symmetrical bending modes, the distribution of amplitudes is symmetrical in relation to the vertical plane passing through the center of the mounted axle, as a pear function, showing a maximum in this plane. In antisymmetric modes, the amplitude distribution is antisymmetric like an odd function, and in the vertical plane of symmetry of the axle, it shows a node.

In both types of own modes, increasing the order leads to the complication of the form of the distribution of amplitudes in the sense of increasing the number of sections with ventre or nodes.

Figures 15 and 16 show the wheel and axle receptance at the axle box for symmetrical excitation both at the level of the wheel treads and at the level of the axle boxes on the frequency range between 10 and 1000 Hz. The resonant frequencies in the case of symmetric excitation are 72 Hz, 254 Hz and 724 Hz.

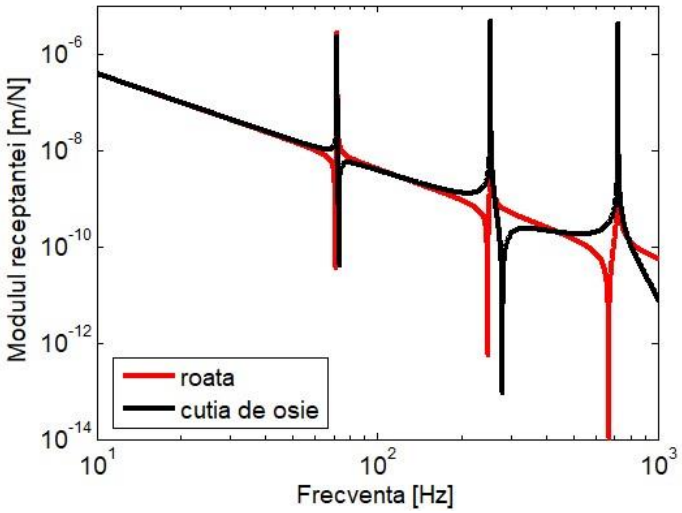


Fig. 15. Wheel and axle receptance at the axle box symmetrical excitation to the tread surface (MEF).

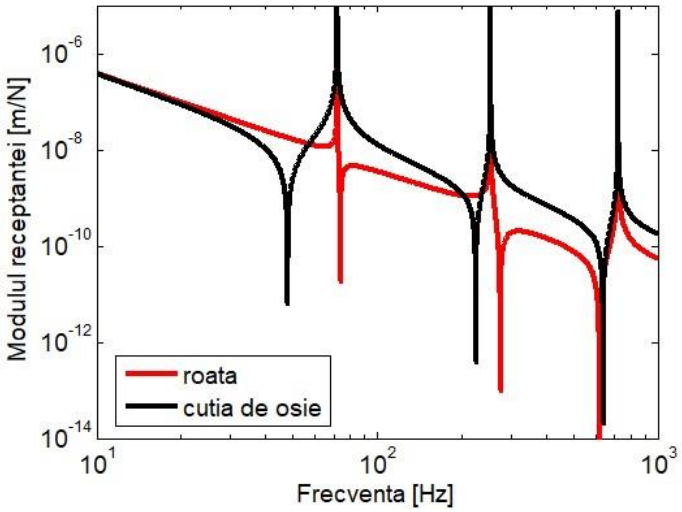


Fig. 16. Receptance of the wheel and axle at the axle box at symmetrical excitation in the axle boxes (MEF).

At the same time, the diagrams in Figures 17 and 18 show the receptances at the level of the wheels and axle boxes when the excitation is antisymmetric applied to the running surfaces (fig. 17) and to the axle boxes (fig. 18). For antisymmetric excitation of the mounted axle, resonant frequencies at 127, 470 and 1045 Hz can be observed.

In general, the diagrams show the same characteristics as observed when using the analytical model, which is why they will no longer be highlighted. There is a very good similarity in the field of low frequencies, up to about. 100 Hz.

Next, attention is focused on the differences that occur in the resonant frequencies of the wheelset. For this, table 2 lists the resonant frequencies of the mounted axle calculated with the two models.

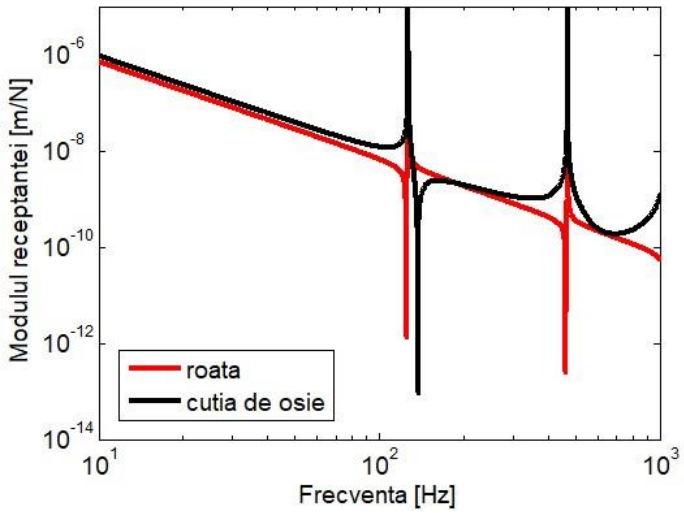


Fig. 17 Wheel and axle receptance at the axle box at antisymmetric excitation at the wheel tread (MEF).

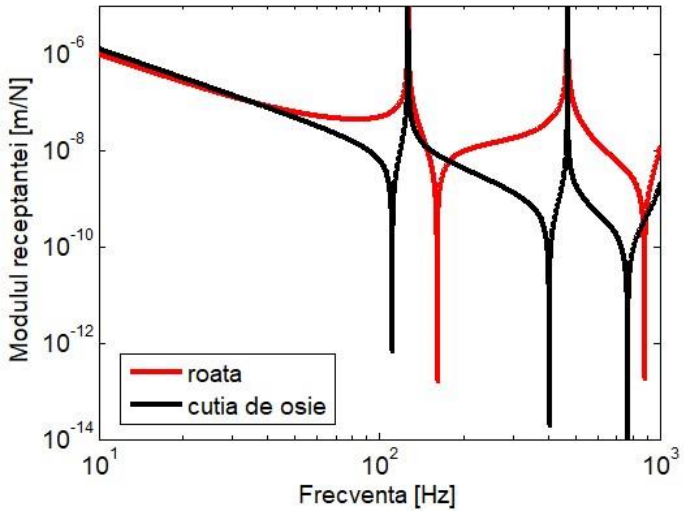


Fig. 18. Wheel and axle receptacles at the axle axle box at antisymmetric excitation at axle boxes (MEF).

It is evident that there are differences between the resonance frequencies calculated with the two models. These differences can be justified by the fact that the analytical model is simpler. It does not take into account a number of effects such as those due to the rotation of the cross-sections of the axle as a result of the shear forces, as well as the effect due to the deformation of the wheels; it is recalled that in the analytical model the wheels are considered rigid bodies.

However, it is important to note that in the case of the first symmetrical bending mode of the wheelset, the resonance frequency has very close values: 72 Hz with the finite elements model and 74 Hz with the analytical model. This result is likely to give consistency to the model with finished elements that will be used in Chapter 5 for the study of vibrations of the rail wheel system.

On the other hand, the variation in the wheel receptance as a function of frequency is similar to that shown in other specialized works [80, 89, 122, 124].

Chapter 5 shows the model for the study of the vibrations of the wheel-rail system based on the non-linear model of the railway presented in Chapter 3 and that of the mounted axle presented in Chapter 4. The two models mentioned are completed with the model of the suspended mass of the bogie to extend the frequency range in the register of low frequencies, as well as with the model of the elastic contact between the wheel and the rail, based on the theory of elastic contact between two solid bodies of the Hertz.

The first part of this chapter is reserved for the assembly of the parts that make up the model proposed in this work. Calculation assumptions are established and linearization of elastic wheel-rail contact is shown.

The second section of the chapter is devoted to the writing of the equations of motion of the model for the permanent harmonic mode. The purpose of this chapter is to calculate the frequency response functions of the quantities that describe this vibration mode.

In the third section, the equations of the random mode are presented, starting from the spectrum of the density of the power of the excitation of the wheel-rail system, or, as it is also called, the spectrum of the density of the quadratic mean. It is stated that by extending the frequency of applicability of the model, the excitation is due on the one hand to the leveling deviations of the roadway, deviations which are caused by the geometric imperfections of the track embankment and which are characterized by long wavelengths, and on the other hand, by the roughness of the treads which are caused by the imperfections of the treads coming from the technological process of manufacture and as a result of wear during the movement; the latter have small wavelengths. An original method of synthesizing the spectrum of excitation power density is presented starting from the spectrum of the power density of the level recommended by the literature and from the spectrum of the limit level of roughness which is included in the rules governing noise tests of railway vehicles.

In the last part of this chapter is presented the comparative analysis of the results on the random vibration mode of the wheel-rail system obtained with the equivalent linear model of the path and its nonlinear model. It is recalled that the nonlinear track pattern refers to the inclusion of the nonlinear characteristics of the rail plates and ballast prism in the dynamic track response by determining the rigidity of the elastic floors of the model according to the static wheel load and the elastic and rigid portions of the characteristics of the rail plates and the ballast prism. Essentially this is a linearized model with non-homogeneous elastic characteristics valid around the equilibrium position of the path under the action of static wheel load.

The modeling of the wheel-rail system in order to study the vertical vibration mode is based on a series of simplifying assumptions that are unanimously accepted in the literature. Thus, it is based on the finding that both the railway vehicle and the taxiway are symmetrical mechanical structures in relation to the median vertical plane. Furthermore, a basic requirement for the operation of railway vehicles is to ensure that static loads on the wheels of the vehicle are balanced in both empty and laden condition. This causes the two wires of the path to be equally strained by the vertical forces that occur at the level of wheel-rail contact during circulation. In those circumstances, it is to be expected that, on the one hand, the uses of the running surfaces of the rails and, on the other hand, the deviations in the geometry of the track will take substantially similar shapes on the two tracks of the track. This results in a first simplifying hypothesis: the vehicle-track road combination is reduced to one half whose separation plane is the longitudinal vertical plane. In other words, in studies on vertical

vibrations, work is being done with a 2D mechanical model that represents 1/2 of the vehicle running on a rail.

The second hypothesis relates to the frequency range in which the vehicle's own frequencies are located and the own frequencies of the wheel-rail system. The vehicle's own frequencies are between 0 and 20 Hz and its vertical vibrations are mainly induced by leveling deviations of the path. These leveling deviations come from the unevenness of the path prism and are characterized by wavelengths ranging from 3 m to 100 - 120 m. For the usual traffic speeds these wavelengths induce low-frequency vibrations, excitating the vibration modes of the vehicle.

The own frequencies of the rail wheel system are more than 40-50 Hz, and the excitations come from the roughness of the running surfaces of the wheels and rails. The wavelengths of the roughness of the treads are less than 3 m and can reach up to several centimeters. The vibration frequencies induced by the wheel-rail system can reach 2 to 3000 Hz.

It follows from the two aspects set out above that the vibrations of the vehicle are decoupled from the vibrations of the train from the wheels of the vehicle when driving on the rails. Corroborating with the first hypothesis, it is inferred that for the study of vibrations at the level of the interface between the wheels and the rails it is sufficient to take into account only the wheel train running on a rail. The influence of the suspended part of the vehicle is reduced to the static load acting on each wheel. By this, it is emphasized that the coupling between the wheels by means of suspension is negligible.

The third hypothesis concerns the coupling between the wheels by means of bending waves that propagate through the rail and which were analysed in detail in Chapter 3. It has been observed that at any frequency, an evanescent wave propagates through the rail, which may or may not be accompanied by a wave of propagation. The frequency domains in which two evanescent waves or an evanescent wave and a propagation wave are propagated through the rail have been determined. At average frequencies the propagation bending waves are attenuated over relatively small distances due to damping. Only in the frequency range of rail resonance on sleepers, which is located at over 800-1000 Hz, propagation bending waves have less attenuation and therefore become efficient over longer distances, thus being able to couple the wheels of a bogie or even a vehicle.

Results obtained with linearized model with homogeneous elastic characteristic

The numerical results on the vibration of the wheel-rail system obtained by means of the equivalent linear track model are given below.

Figure 8 shows the modules of the receptances of the wheel-rail system, namely the receptance of the rail at the point of contact with the wheel (the section where the harmonic excitation force acts) calculated for the two loading situations, the empty wagon/wagon loaded (see Table 4), the receptance of the axle next to the wheel at symmetrical excitation on the running surface of the wheels, as well as the receptance of the elastic wheel-rail contact, also for the two wagon loading states. The calculations were carried out without taking into account the damping of the railway.

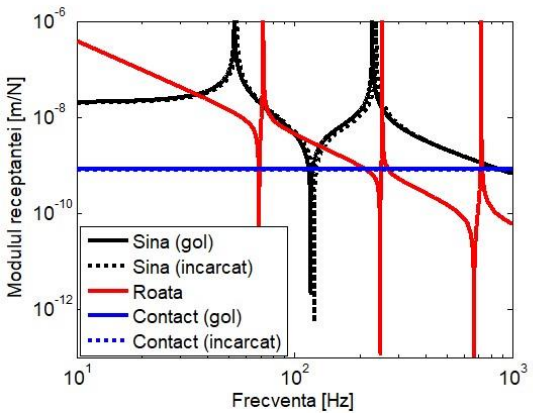


Fig. 8. Receptances of the wheel-rail system.

As regards the receptance of the rail, the difference between the two load states reflected by the wheel load and by the different values of the two elastic floors of the linear model equivalent to the track is observed. If the track model corresponds to the case of the wheel load for the empty wagon, the receptance of the rail at low frequency is higher because the rigidity of the path, reflected either by the path module or by its rigidity, is lower (v. Table 4). The resonant frequencies are at 53,2 Hz and 228,3 Hz for the static wheel load of 51,250 kN and 54,5 Hz and 238,5 Hz respectively for the static wheel load corresponding to the loaded state of the wagon.

The anti-resonance frequency which stands at 118.9 Hz is also important if the wheel load is 51,250 kN for the empty wagon and 123.7 Hz for the loaded wagon.

It can be concluded that the small differences between the two track receptance results are due to the fact that, specific to long-distance coaches such as the one for which the numerical analysis was carried out, the difference between the empty state and the loaded state is small, in this case the difference is 13 %.

The axle receptacles next to the wheel at symmetrical excitation applied to the treads was presented in Chapter 4 using the finished elements model (see Fig. 15). However, the main results that help to understand the dynamic mode of the wheel-rail system are recalled: the resonant frequencies of the wheelset within the frequency range considered (10–1000 Hz) are at 72,1 Hz, 254,1 Hz and 724,7 Hz, and the anti-resonance frequencies at 71 Hz, 248 Hz and 670 Hz.

The graph in Figure 8 also shows the receptacity (elasticity) of the contact between the wheel and the rail, calculated as shown on the basis of Hertz's nonlinear model.

The stiffness of the contact was calculated considering that the wheel has a profile S 78 with a radius of curvature on the tread of 500 mm, and the rail has the specific profile UIC 60 at which the running surface of the rail has a radius of 300 mm. Applying the calculation relationships, the value of the contact stiffness kH = 1,192 GN/m, respectively of the receptance, $\square_H$ = 8,391·10-10 m/N for the empty wagon and kH = 1,242 GN/m and $\square$H = 8,052·10-10 m/N for the loaded wagon is obtained.

It is noted that the contact receptance is much lower than the track receptance at the point of contact with the wheel and the axle receptance at the wheel in the low frequency range, but becomes comparable to the rail receptance at high frequency, in the vicinity of the 1000 Hz threshold.

It is therefore to be expected that in the field of high frequencies, the receptance of contact between the wheel and the rail will play an important role in terms of dynamic mode.

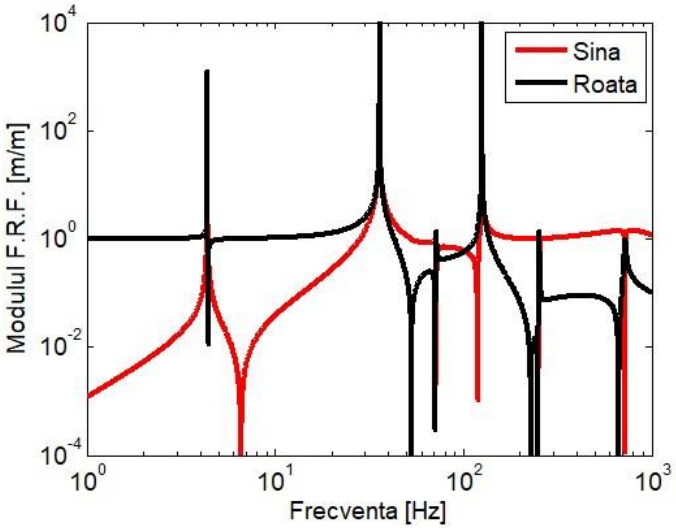


Fig. 9. Frequency response function for the rail in the wheel contact and wheel contact section.

Figure 9 shows the frequency response function of rail movement in the wheel contact section and wheel displacement for an extended frequency range covering 1–1000 Hz. Frequencies below 10 Hz have also been taken into account to highlight the resonant frequency due to the suspended mass of the bogie and the primary suspension. The case of the empty wagon was considered.

It is established that the dynamic mode is characterized by a series of three resonances occurring at frequencies of 4,4 Hz, 36,0 Hz and 126 Hz. The first resonant frequency is due to the suspended mass of the bogie on the primary suspension. The second and third resonances are the result of the interaction between the wheel and the rail. These frequencies are located in the areas where stationary evanescent waves propagate through the rail.

Indeed, analyzing the track receptance results in the wheel contact section in the light of the results obtained in Chapter 3, it is observed that the first range of stationary evanescent waves comprises frequencies less than 53,2 Hz – this range occupies the range of frequencies lower than the first resonant frequency. The second area in which evanescent waves stationary through the rail propagate is between the anti-resonance frequency, which, for the parameters of the equivalent linear model of the wagon in the empty state, is at 118.9 Hz, and the second resonant frequency (228.3 Hz).

Anti-resonance modes at the following frequencies may also be signalled: the wheel at 4,4 Hz, 53,2 Hz, 71 Hz, 228,3 Hz, 248 Hz and 670 Hz, and the rail in the wheel contact section at 6,6 Hz, 72,1 Hz, 118,9 Hz, 254,2 Hz and 724,1 Hz.

With regard to the amplitude of the frequency response, it is noted that in the range of frequencies lower than the first resonant frequency of the wheel-rail system, the amplitude of the wheel vibration is greater than that of the rail in the wheel contact section. This was explained by the fact that in this frequency range the wheel receptance is greater than the track receptance in the wheel contact section as can be seen in Figure 8. Moreover, the point of intersection of the graphs of the two receptances practically corresponds to the first frequency of resonance. The receptance of the wheel being larger than that of the rail, it follows that in

dynamic (harmonic) mode the wheel is more 'elastic' than the rail and, as a result, takes over the unevenness imposed by the presence of roughness on the tread, while the rail, which is less elastic, tends to remain motionless, that is, it has much smaller displacements compared to those of the wheel. On the diagram in Figure 9, it is noted that the frequency response function of the wheel tends to take the unit value – the movement of the wheel is practically equal to the relative wheel-rail displacement due to roughness.

In the field of high frequencies, higher than the first resonant frequency of the wheel-rail system, with the exception of the areas around the resonance frequencies of the axle mounted from 254,1 Hz and from 724,1 Hz, as well as the area where the rail shows the anti-resonance mode at 118,9 Hz, it is observed that the dynamic mode is more intense at the level of the rail. In this frequency range, the track receptance is higher than that of the wheel, as shown in Figure 8, which explains why the rail takes over the movement required by the roughness of the treads; the value of the frequency response function of the rail is located around the unit value. This aspect is very well highlighted at frequencies higher than the second resonant frequency of the wheel-rail system. On the other hand, in the resonance zones of the mounted axle as well as in the anti-resonance frequency of the rail, the receptance of the wheel is higher, which makes it follow the level of roughness of the tread.

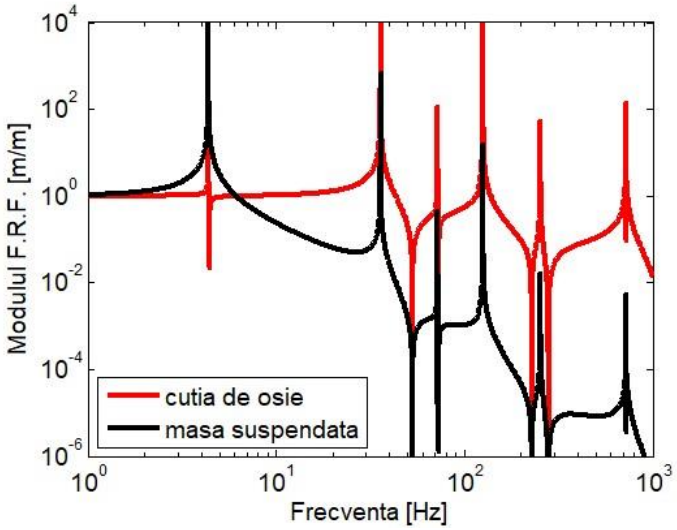


Fig. 10. Frequency response function for axle axle to axle box and suspension mass of bogie.

Figure 10 shows the frequency response functions of the axle next to the axle box and the suspended mass of the bogie. The dynamic axle mode next to the axle box is similar to that of the wheel due to the proximity between the axle spindle and the wheel riding area, and therefore the response function next to the axle box is practically identical to that of the wheel.

As for the dynamic mode of the suspended mass of the bogie, it is more intense in the range of the low frequencies around the first resonant frequency which is, as we have seen, at 4.4 Hz. At frequencies of 1-2 Hz, it is observed that the two frequency response functions take values close to the unit, which shows that the two bodies (the axle box and the suspended mass of the bogie) vibrate together. At higher frequencies, the axle box continues to take over the imposed displacement, while the vibration of the suspended mass of the bogie is amplified by the resonance effect. At frequencies greater than 6-7 Hz, the phenomenon of vibration filtration introduced by the primary suspension occurs, which causes the vibration of the suspended mass of the bogie to decrease as the frequency increases.

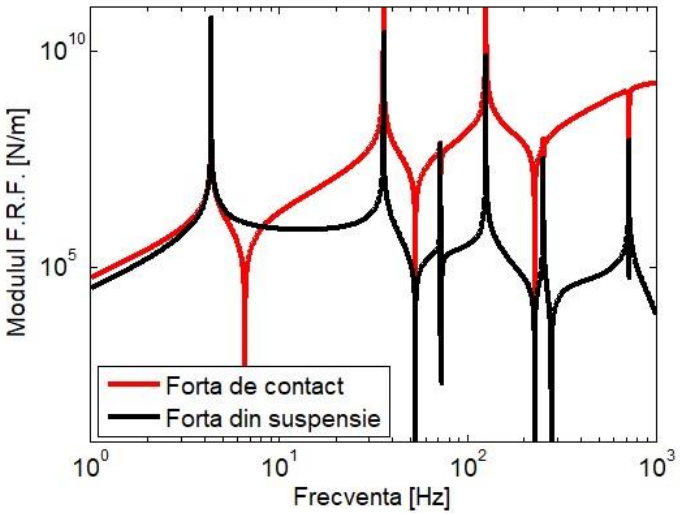


Fig. 11. Frequency response function for the contact force and the force in the primary suspension.

Figure 11 shows the frequency response functions of the dynamic red-strand contact force and the force in the primary suspension. The force in the primary suspension is greater than the dynamic component of the contact force only in a small frequency range located after the resonance of the suspended mass of the bogie. For the rest, the frequency response function of the dynamic component of the contact force is dominant.

Clearly, the frequency response functions of the two forces are dominated by the peaks recorded next to the resonant frequencies of the wheel-rail system. On the other hand, the correspondences that can be established between the dynamic contact force and the dynamic mode of the wheelset and rail must also be indicated (see Fig. 8). Thus, the frequency response function of the dynamic component of the contact force shows a minimum of anti-resonance type at the following frequencies: 53,15 Hz, 72,1 Hz, 228,3 Hz, 254 Hz and 724 Hz. Comparing the results obtained with those shown in Figure 8, the following conclusions are drawn: the dynamic contact force becomes minimal at the resonance frequencies of the rail (53,15 and 228,3 Hz) and in the vicinity of the wheel's anti-resonance frequencies (71 Hz, 248 Hz and 670 Hz). Also, the wheel-rail contact force is minimal and at the resonant frequency of the system composed of the primary wheel-suspension - the suspended mass of the bogie considered as a system with two degrees of freedom of which only one is the degree of elastic freedom.

At the same time, local maximum values of the same frequency response function can also be reported at 71.7 Hz, 253.8 Hz and 723 Hz without any correlation being made with the wheel receptance or rail receptance. These peaks appear only because they precede the anti-resonances and therefore do not have a certain meaning.

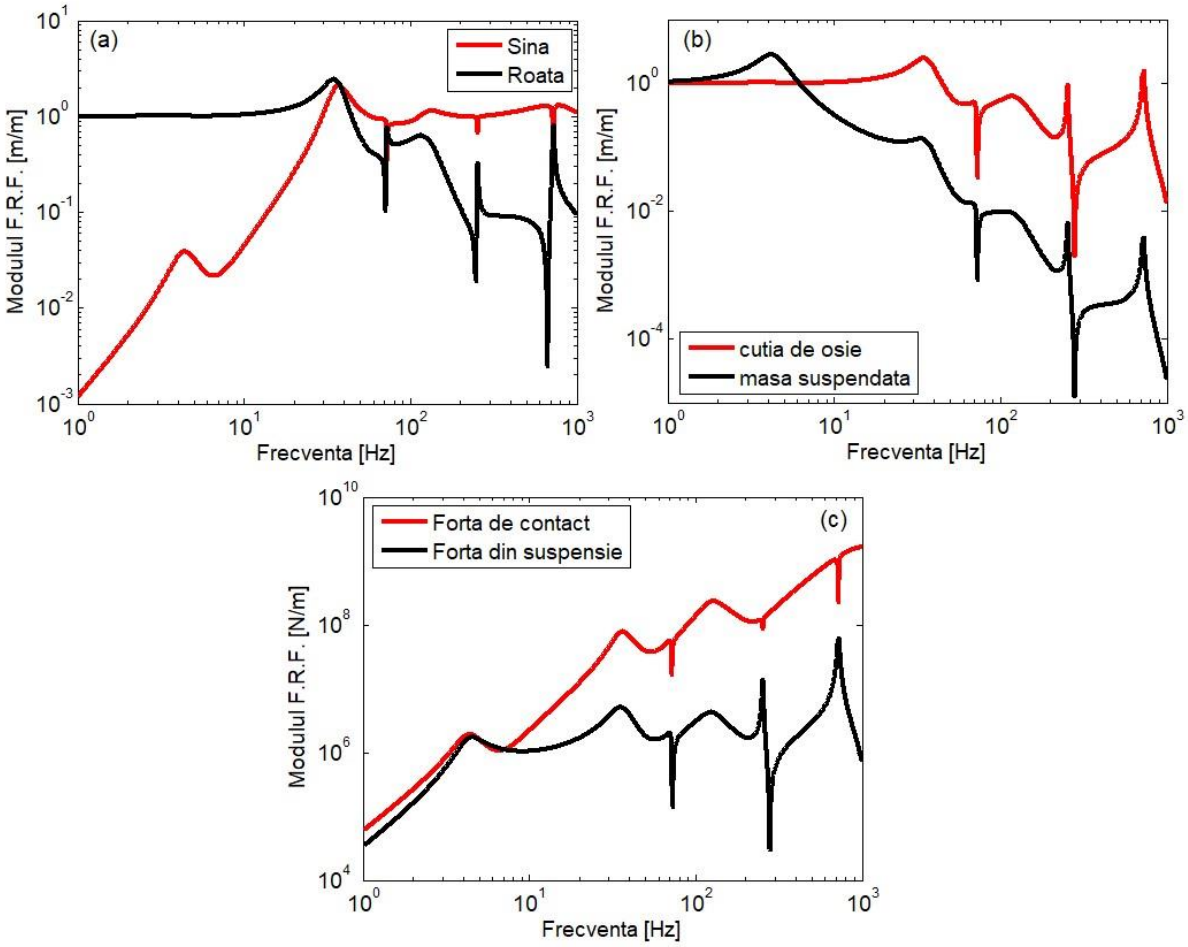


Fig. 12. Frequency response functions – MLCEO with viscous damping

Figure 12 shows the frequency response functions obtained with the viscous damping MLCEO.

Damping influences the frequency response functions of the linear equivalent model in the frequency ranges around resonances and anti-resonances. Although the values of the degrees of depreciation are moderate, it is found that under certain conditions, depreciation can completely blur the existence of either resonances or anti-resonances.

For example, at the wheel-rail level, it can be seen how the resonance of the system at 4.4 Hz has completely disappeared from the response of the wheel or axle box (see Fig. 12 a and b). This resonance can be detected more clearly only at the suspended mass of the bogie, as well as at the force response in the primary suspension. A second example concerns the anti-resonance that appears on the wheel frequency response diagram at 53,1 Hz or the rail anti-resonance from 118,9 Hz. In this regard the contribution comes from both the damping of the path and the structural damping of the axle material.

The analysis of the charts in Figure 12 reveals a number of characteristics of the wheel-rail system response. First of all are the three resonant frequencies that have been highlighted above. Low-frequency resonance (4.4 Hz) affects practically only the response of the suspended mass of the bogie. The other two resonances are the result of the interaction between the mounted axle and the rail and influence virtually all the response functions of the system. The greatest influence can be observed at the average resonance frequency, from 35.5 Hz, where an amplification of both the wheel vibration and the rail can be identified; they have comparable amplitudes. This resonance makes the difference between the way the two components of the

wheel-rail system vibrate: at lower frequencies, the vibration of the wheel is greater than the vibration of the rail in the wheel contact section, and at higher frequencies, the dynamics of the wheel-rail system is dominated by the vibration of the rail. This is how it is that the response to the third resonance (126 Hz) is practically noticeable at the level of the rail. It is true that the vibration of the wheel also amplifies at this resonant frequency, but its size is much smaller than that of the rail in the contact section with the wheel.

With regard to the calculated forces, i.e. the contact force and the force in the primary suspension, the frequency response highlights the fact that the two forces are close only in the resonance range of the suspended mass. For the rest, the frequency response of the contact force is much greater, and the difference increases practically continuously with the frequency of excitation.

The numerical results of the frequency response functions obtained with the MLCEO taking into account the hysteretic depreciation of the path model are shown in Figure 13.

The results obtained with the hysteretic depreciation model are similar to those achieved by applying the viscous damping model. From the frequency response diagrams shown in Figure 13, the characteristic forms of the variation of the transfer functions for the movements of the bogie frame, wheel and rail, as well as of the two forces – from the wheel-rail interface and the primary suspension – can be recognised. Local peaks that signal the presence of resonant modes appear, as well as the minimums characteristic of anti-resonance modes.

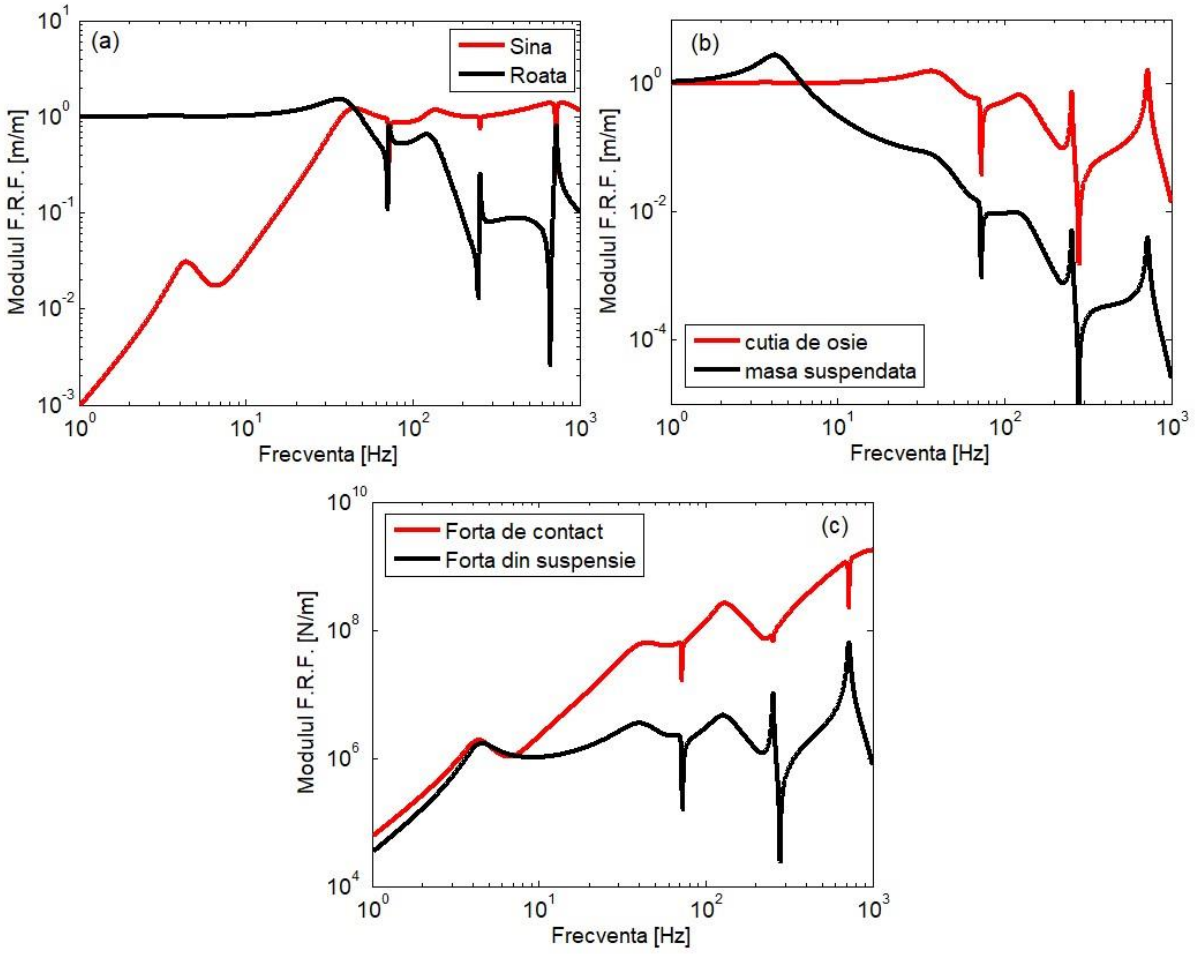


Fig. 13. Frequency response functions – MLCEO with hysteretic damping (a) wheel and rail; (b) the axle box and the suspended mass of the bogie; (c) the contact force and force in the primary suspension.

It should be noted that those peaks do not correspond to the same frequencies. For example, the frequency response functions of the two calculated forces have highs at: 4.4 Hz, 36.6 Hz and 129.2 Hz for viscous damping and at 4.4 Hz, 44.8 Hz and 131.9 Hz for hysteretic damping. It is noted that in the case of the hysteretic damping model, the resonant peaks corresponding to the wheel-rail interaction appear at higher frequencies than those obtained with the viscous damping model.

Another aspect that differentiates the two models relates to the ratio of the different representative sizes and from this point of view are interesting the values of the frequency response function calculated at the resonance frequencies due to the wheel-rail interaction. In order to illustrate that aspect, account must be taken, on the one hand, of the ratio between the values of the frequency response function to the two values of the resonant frequency and, on the other hand, of the ratio between the depreciations of the two elastic floors of the railway model.

The allure of the power density of the contact force retains the 'imprints' of the anti-resonance modes due to the resonance of the suspended wheel-mass system, the low and high resonance of the rail receptance, as well as the anti-resonances of the axle, with the specification that the effect produced by the low resonance of the rail receptance is cumulated with that of the first anti-resonance of the axle covering the frequency area 50-75 Hz.

On the other hand, it is possible to identify the effect of excitation which has a higher amplitude at lower frequencies to which long wavelengths correspond, namely that the three peaks have comparative amplitudes, unlike the situation shown in the diagram of the frequency response function in which the three peaks were in ascending scale with large gaps between them.

The hysteretic damping model does not fundamentally change the behavior of the wheel-rail system. The allure of the spectral power densities of the rail accelerations in the wheel, wheel and suspended mass contact section, as well as the allure of the spectral power densities of the contact force and the suspension force are similar to those resulting from the application of the viscous damping model. Some differences may be reported. For example, the peak acceleration of the suspension mass of the bogie is greater than those of the wheel and rail at the resonance of the axle on the rail in the case of hysteretic damping. The results obtained with the viscous damping model show that this tip has a lower 'height' than the other two.

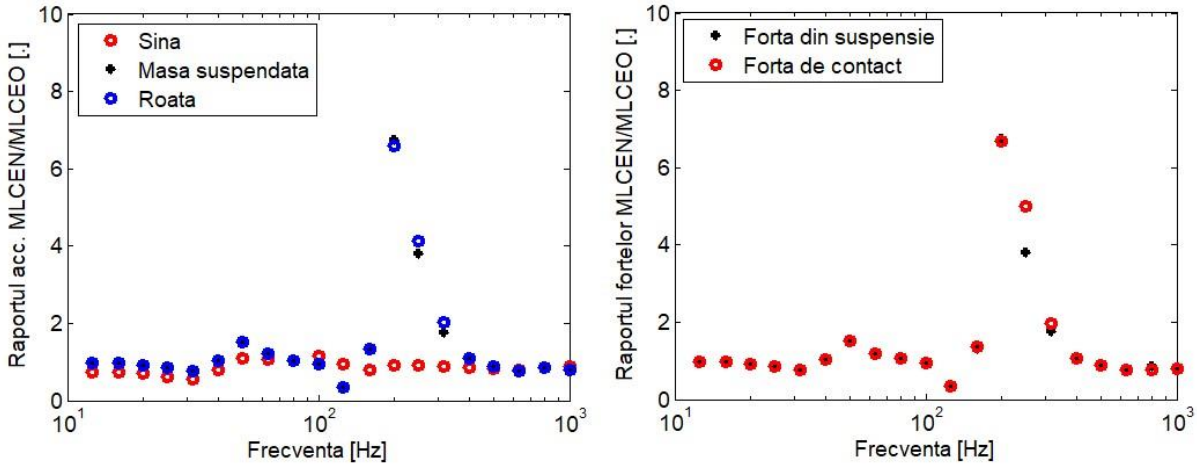


Fig. 23. Ratio of effective values calculated with MLCEN to effective values calculated with MLCEO (model with viscous damping): (a) acceleration of the rail, wheel and suspended mass; (b) the contact force and the force in the suspension;

The analysis of the two figures leads to the conclusion that regardless of the type of damping model adopted for the track, the differences between the results offered by MLCEN and MLCEO are similar. Thus, as regards the acceleration of the rail at the point of contact with the wheel, the track model with homogeneous characteristic leads to values higher than those obtained by the model with non-homogeneous characteristic and this aspect can be noticed on almost the entire frequency range investigated. The exception to this observation is the results obtained at frequencies between 40 and 100 Hz, where the rail acceleration calculated with MLCEN is greater than that calculated with MLCEO.

At the wheel, the results are different, in the sense that there are frequency areas where the acceleration calculated with MLCEN is higher than that calculated with MLCEO, so that in other frequency ranges the situation is changed.

And in terms of contact force and force in the primary suspension, noticeable differences can be noted between the spectral power densities calculated with the two models. The differences are not only quantitative, but also qualitative, in the sense that while the spectral density calculated with one model has a local maximum, the spectral density calculated with the other model has a local minimum. These aspects can be easily ascertained in the frequency range between 100 and 300 Hz.

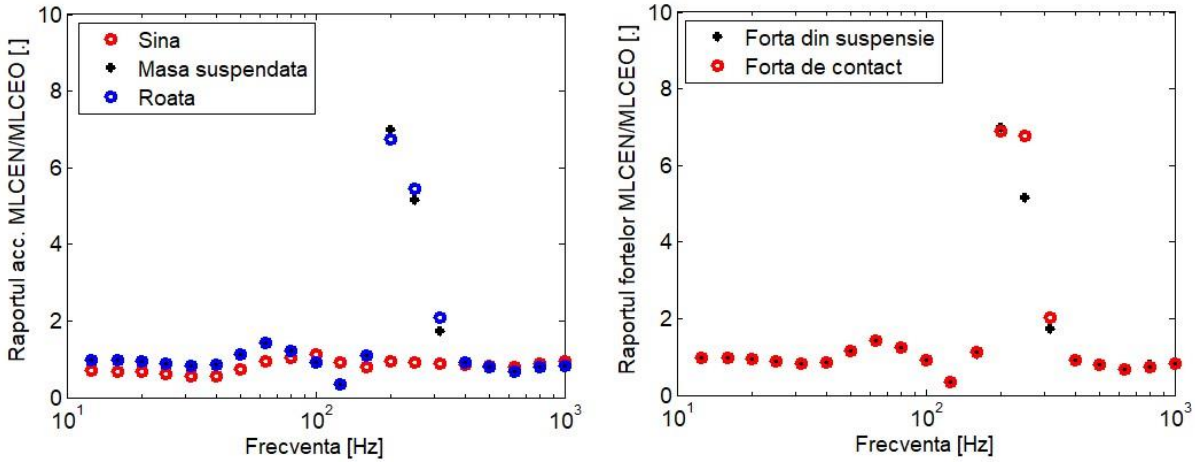


Fig. 24. Ratio of effective values calculated with MLCEN to effective values calculated with MLCEO (hysteretic damping model): (a) acceleration of rail, wheel and suspended mass; (b) the contact force and the force in the suspension;

The comparison picture between MLCEN and MLCEO models is completed by digrams in figures 23 and 24 showing the ratio of the effective values calculated with the two models for the intervals of 1/3 octave between 12,5 Hz and 1000 Hz. Rail acceleration calculated with MLCEN is approx. 54 % and 78 % of that calculated with the MLCEO in the 1/3 ranges with the central frequency between 12,5 Hz and 40 Hz. Between 50 Hz and 125 Hz, the rail acceleration calculated with MLCEN shall be close to that given by the MLCEO with variations between 0,96 and 1,09. For the rest, the rail acceleration obtained with MLCEN is between 0.79 and 0.92 of that calculated with MLCEO.

The differences are much greater in terms of the effective acceleration of the wheel and the suspended mass of the bogie, or in the effective value of the contact force or force in the primary suspension. Thus, the effective values of these sizes can be almost 7 times higher when calculated with MLCEN compared to those calculated with MLCEO. These maximum differences are recorded in the range of 1/3 octave centered at 200 Hz. Conversely, at 125 Hz, the ratio of the effective MLCEN-MLCEO values is between 0,33 and 0,35.

Larger differences are recorded at the following central frequencies: 31.5 Hz, the ratio of effective values is 0.76, at 50 Hz, it is 1.52, at 250 Hz, it is 3.8, at 315 Hz, it is 1.75, and between 500 and 1000 Hz the ratio is between 0.75 and 0.87.

In Chapter 6 are presented the experimental tests carried out in order to validate the model proposed in this work. The experimental tests were directly aimed at measuring the vertical acceleration at the axle box level from a Minden Deutz bogie of a 19-55 series passenger wagon at different traffic speeds.

Part of the test results together with a number of original interpretations in relation to the experimental data were published in papers [29-33].

The validation of the model is achieved by comparing the results obtained from the acceleration measured at the axle boxes of the bogie at a certain running speed and the numerical results calculated on using the theoretical model of the wheel-rail system.

In order to carry out the acceleration measurements, an experimental system specially designed for this purpose was carried out, which is shown in Figure 3 in the form of a block diagram [31].

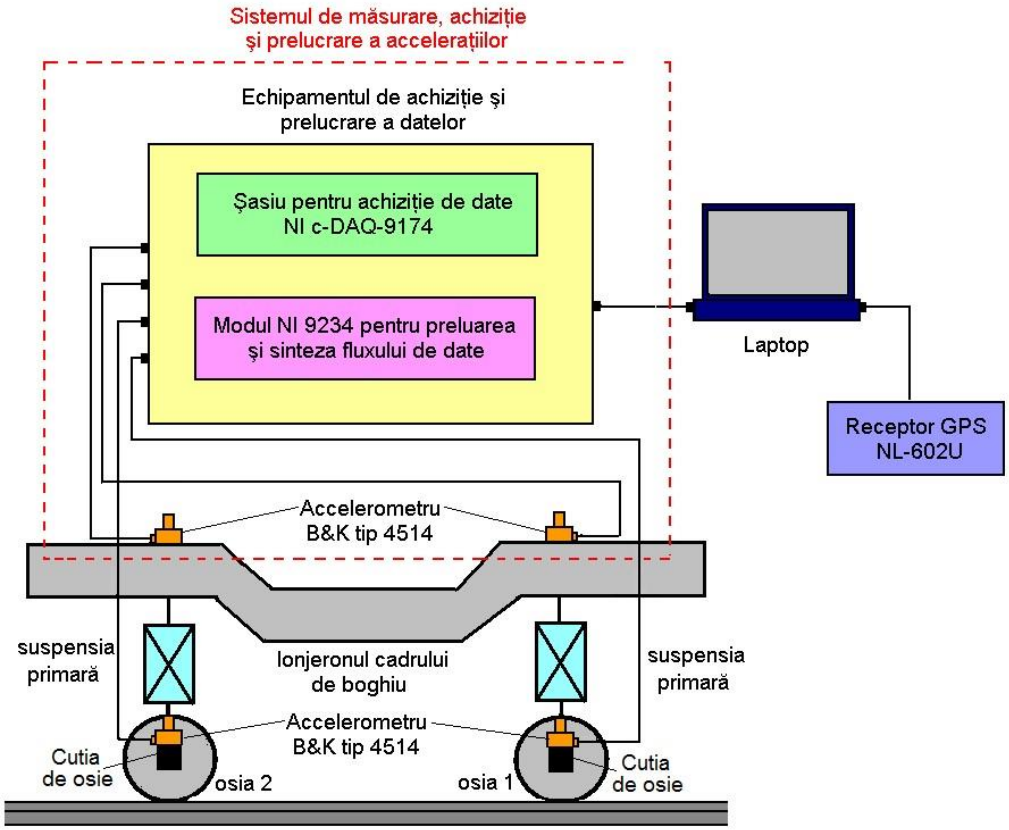


Fig. 3. Block diagram of the system for measuring bogie acceleration and speed of movement [31].

The system is designed to measure the acceleration at four points of the bogie and to purchase and process the electrical signals corresponding to the measured accelerations.

At 137 km/h, the effective acceleration at axle boxes is 2.15 g at the first axle and 2.08 g at the second axle. The effective acceleration of the bogie frame is 1.05 g above the first axle and 1.22 g above the second axle.

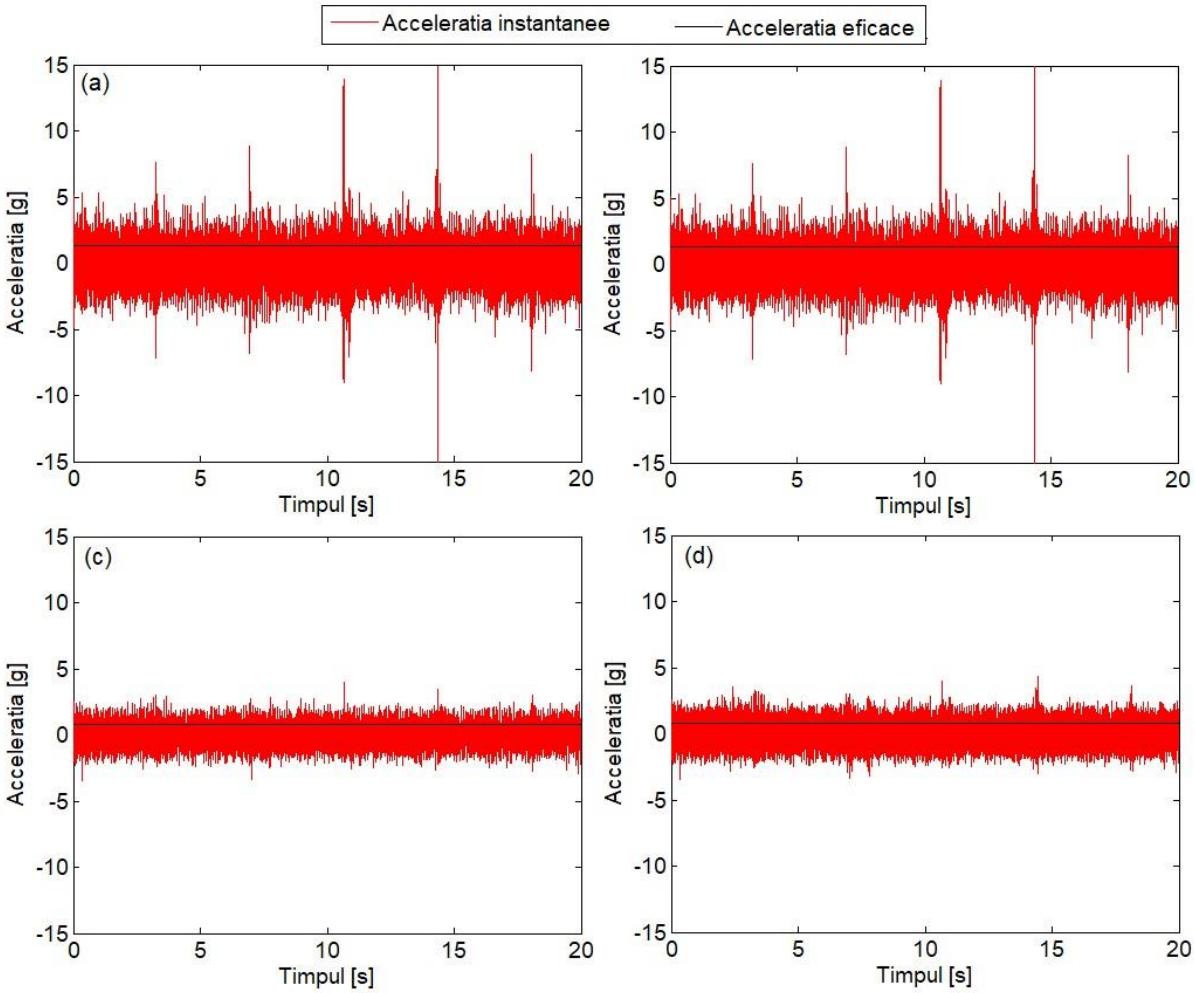


Fig. 15. Bogie acceleration at 117 km/h: (a) axle box 1; (b) axle box 2; (c) the bogie frame above axle 1; (d) the bogie frame above axle 2.

It should be noted that axle 1 on the 117 km/h run, on the return route, corresponds to the second axle to the 137 km/h traffic, when the test train was travelled during the journey. This aspect is explained by the fact that in Straulesti station the test wagon was not turned, but only passed from line 1 to line 2, without changing the orientation. In other words, axle 1, at the return journey (speed 117 km/h), means the second axle in the direction of travel. Similarly, axle 1 on the path means the front axle. Having these things clarified, it can be seen that at the level of the axles, the acceleration is higher at the front axle in the direction of travel, and in terms of the bogie frame, the acceleration is higher above the rear axle.

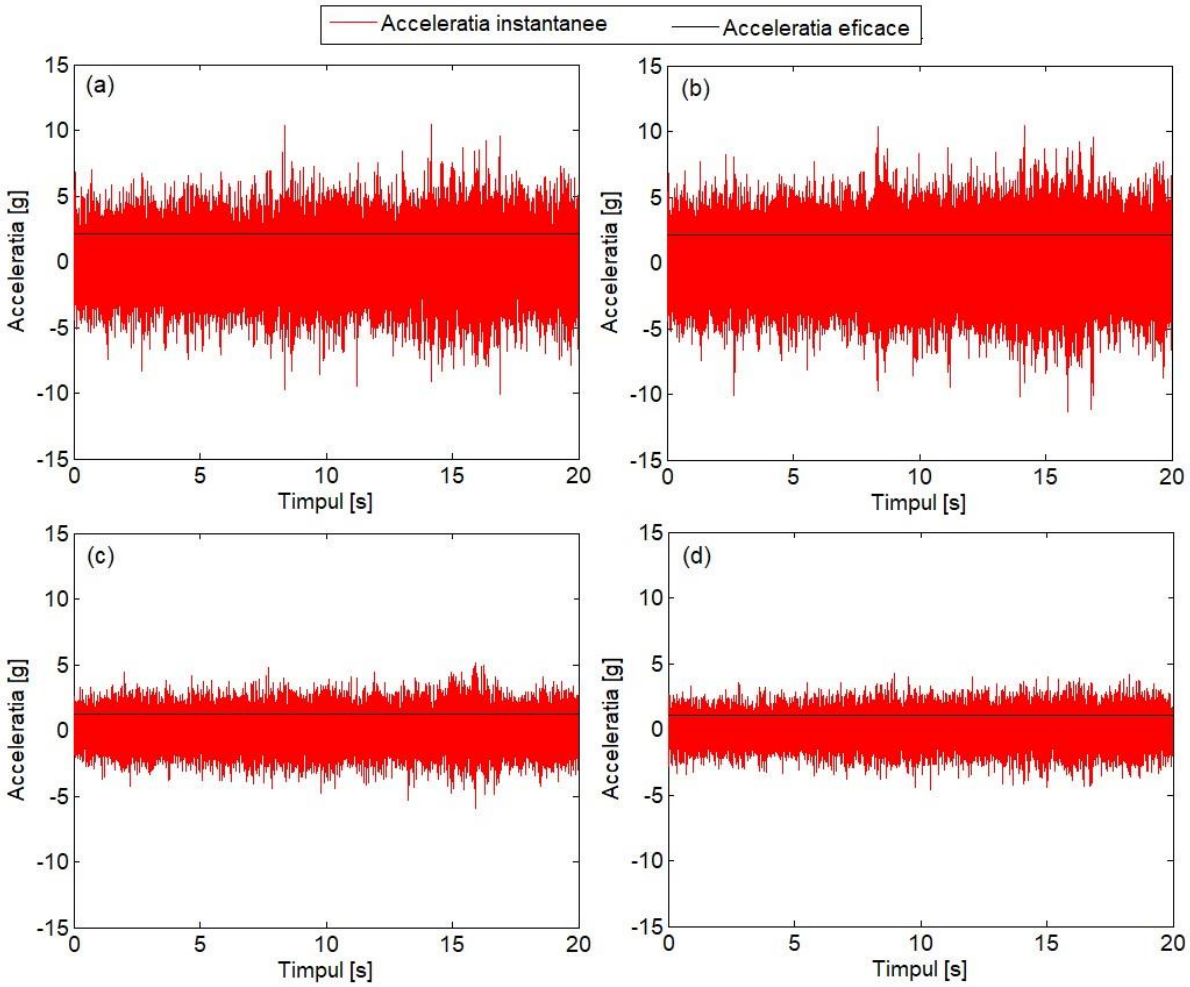


Fig. 16. Bogie acceleration at 137 km/h: (a) axle box 1; (b) axle box 2; (c) the bogie frame above axle 1; (d) the bogie frame above axle 2.

Another important aspect highlighted by the acceleration measurements is that the acceleration size is larger at the level of the axle boxes than at the bogie frame, which is explained by the filtering effect that the primary suspension of the bogie introduces.

On the other hand, it is found that effective acceleration at both the axle boxes and the bogie frame increases with speed. Indeed, effective acceleration increases by 55-58% in bogie axle boxes and 42-61% in bogie frame.

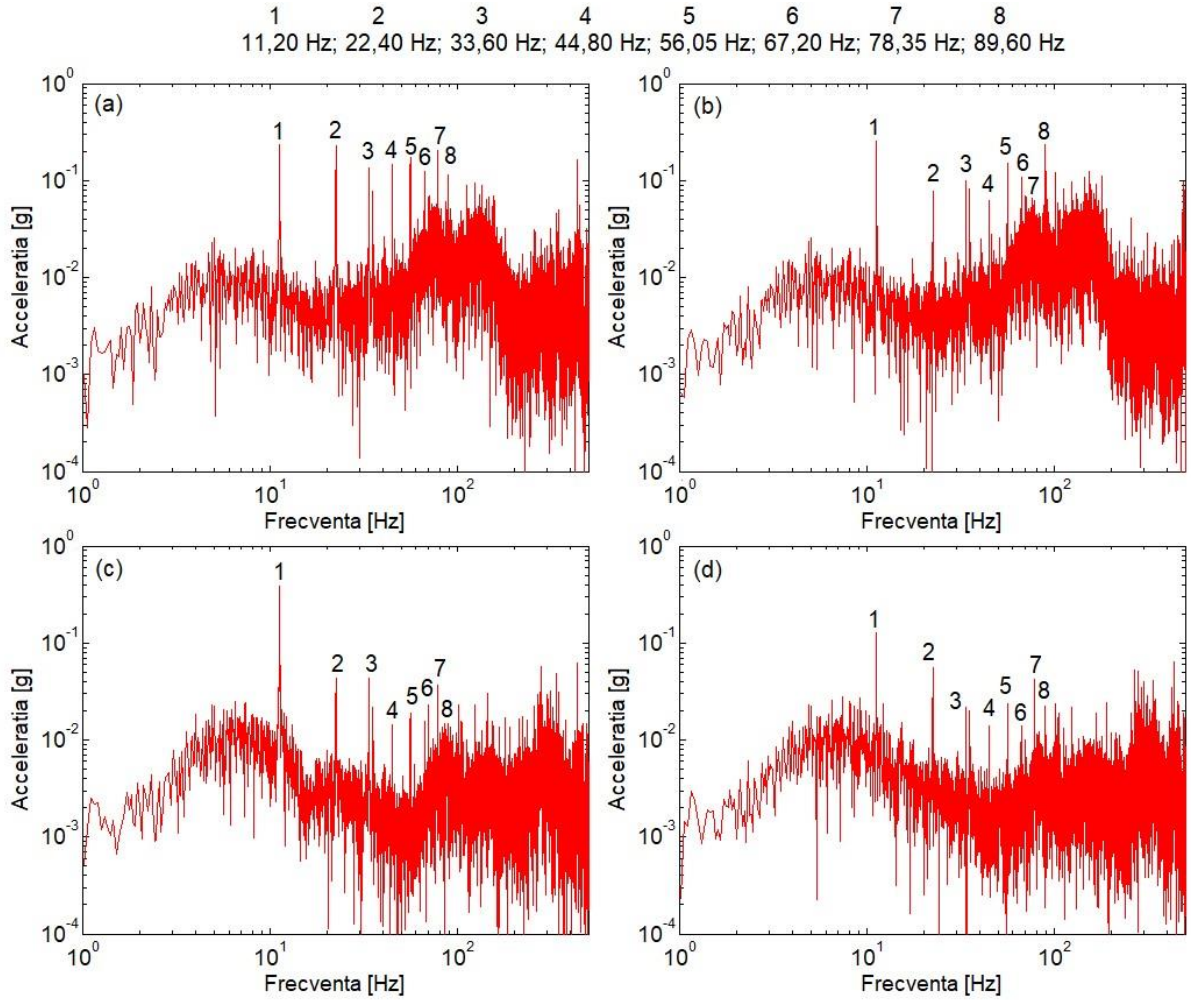


Fig. 17 Acceleration amplitude spectra at 117 km/h: (a) axle box 1; (b) axle box 2; (c) the bogie frame above axle 1; (d) the bogie frame above axle 2.

The throttle spectra have similar shapes both at the level of the axle boxes and at the level of the bogie frame. An intensification of the vibration mode at frequencies between 4-8 Hz can be observed, followed by a decrease in the amplitude of the acceleration, which in the axle boxes reaches a minimum at approx. 20-30 Hz, and at the bogie frame reaches a minimum of about. 40-60 Hz. Around the frequency of 100 Hz can be identified another frequency band in which an intensification of the vibration mode is observed.

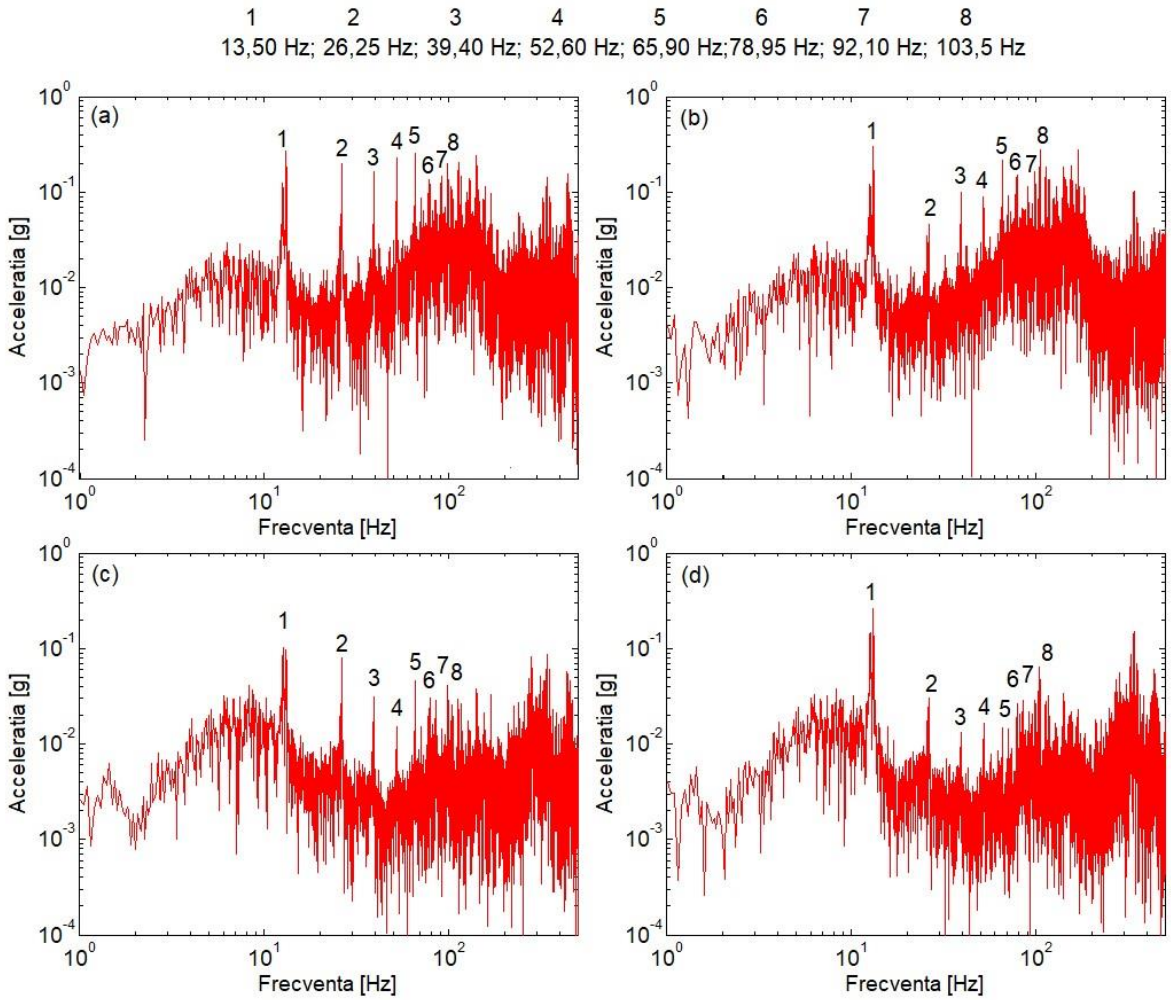


Fig. 18. Acceleration amplitude spectra at 137 km/h: (a) axle box 1; (b) axle box 2; (c) the bogie frame above axle 1; (d) the bogie frame above axle 2.

Another common feature of the acceleration amplitude spectra is that a series of peaks appear on all spectra that are recorded at frequencies that form an arithmetic progression. Indeed, at the acceleration spectra calculated for the speed of 117 km/h, at least 8 peaks are observed whose frequencies are: 11,20 Hz, 22,40 Hz, 33,60 Hz, 44,80 Hz, 56,05 Hz, 67,20 Hz, 78,35 Hz and 89,60 Hz. Also, at the acceleration spectra determined at 137 km/h, the peaks are at the following frequency series: 13,50 Hz, 26,35 Hz, 39,40 Hz, 52,60 Hz, 65,90 Hz, 78,95 Hz, 92,10 Hz and 103,50 Hz.

In order to identify the source of these acceleration peaks, their wavelength must be established. It is known that the wavelength of a periodic defect can be calculated as the ratio between the running speed (in m/s) and the frequency at which the vibration induced by that defect occurs.

It is noted that the wavelengths calculated at the two running speeds are very close for each component. A relatively larger difference is found in the first and last component, but also in these cases the relative error is less than 3%.

As indicated in § 5.2, the wheel-rail system model is synthesized by the frequency response functions that connect the disruptive size of the system to its response. In the second stage, these frequency response functions are applied in reverse and the disruptive size, i.e. the

amplitudes of the tread defects, are calculated, depending on the response of the system in the form of acceleration measured at speed *V1*.

The third stage is also a calculation stage, in which this time the frequency response functions are used in direct form. In this way, calculate the accelerations of the bogie at speed v_2 starting from the amplitudes of the tread defects obtained at the previous stage.

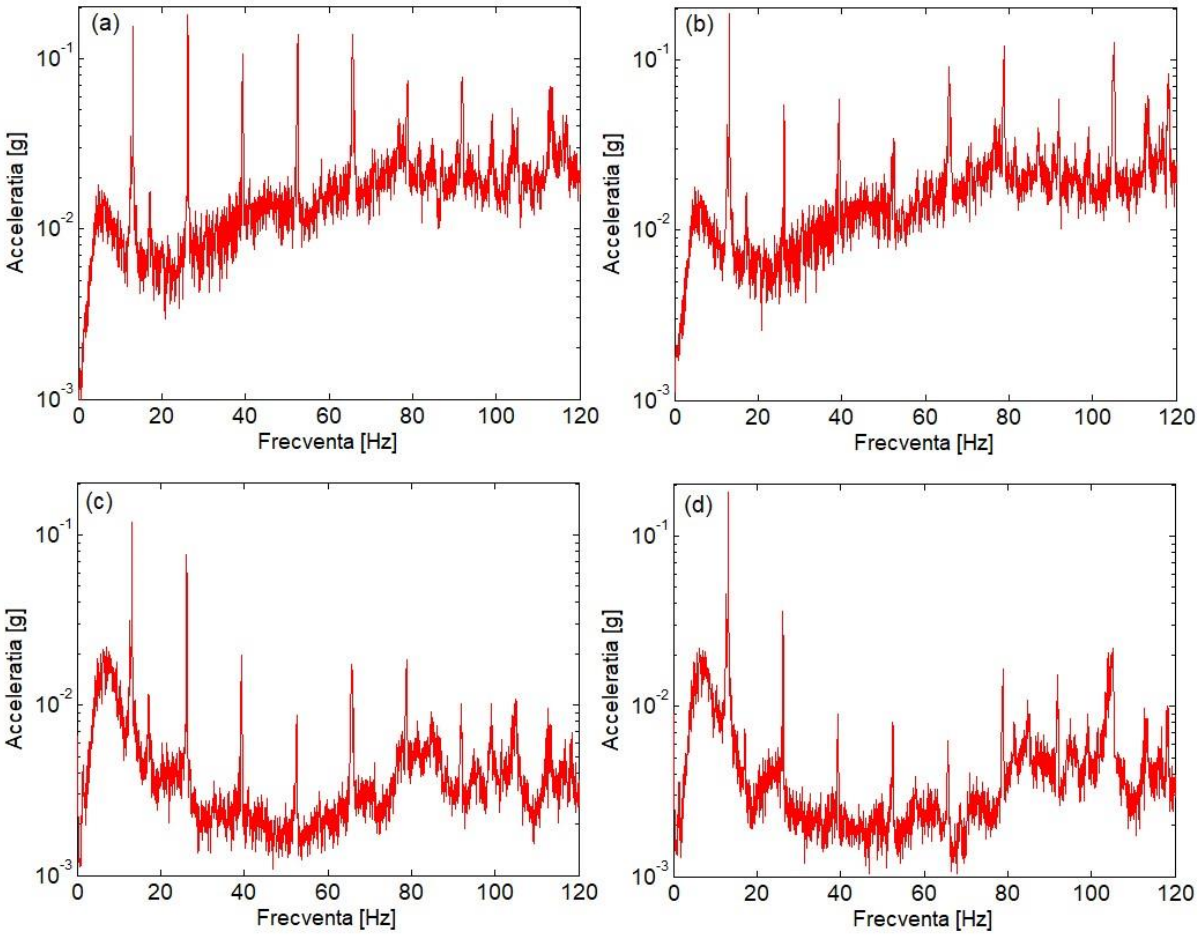


Fig. 23. Effective acceleration spectra measured at 137 km/h: (a) axle 1; (b) axle 2; (c) bogie frame above axle 1; (d) the bogie frame above axle 2.

As will be seen below, the two steps are cumulative in the sense that there is no need to calculate the defects of the treads, which is why they are framed by a broken line border.

The last step of the procedure is to compare the accelerations measured at speed v_2 with the accelerations calculated for the same speed.

Moving on to the first stage of the procedure, 12 acceleration records at a speed of 137 km/h and a further 12 recordings at a speed of 117 km/h were selected to calculate a statistic on the throttle spectra.

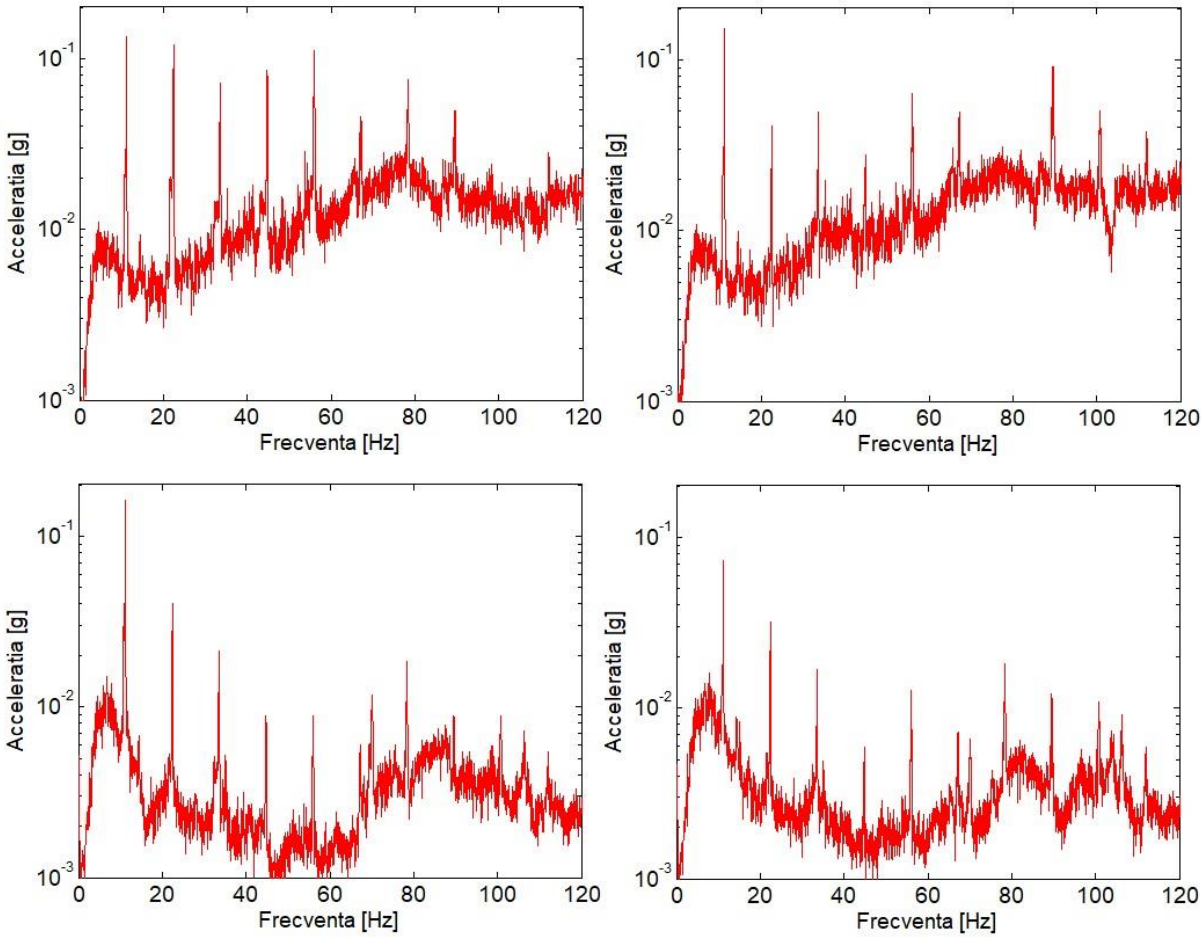


Fig. 24. Effective acceleration spectra measured at 117 km/h: (a) axle 1; (b) axle 2; (c) bogie frame above axle 1; (d) the bogie frame above axle 2.

Figures 23 and 24 show the spectra of effective acceleration determined from measurements at speed v_1 = 137 km/h and at speed *V2* = 117 km/h. Spectra were determined by calculating first for each spectral component the quadratic mean of acceleration from all 12 recordings, and then the effective value.

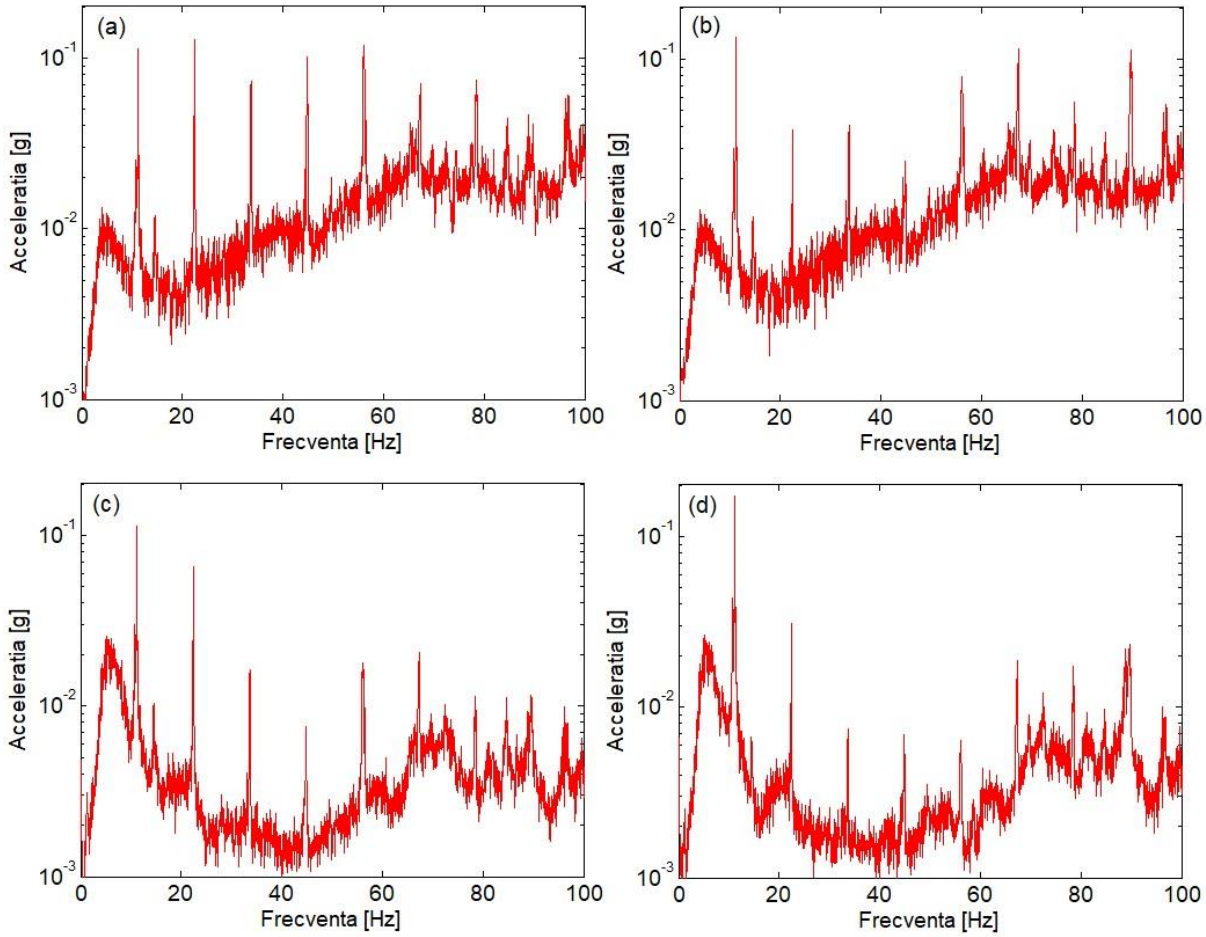


Fig. 29 Effective acceleration spectra at 117 km/h obtained by calculation: (a) axle 1; (b) axle 2; (c) bogie frame above axle 1; (d) the bogie frame above axle 2.

Figure 29 shows the effective accelerations calculated at speed v_2 =117 km/h starting from the accelerations measured at speed v_1 = 137 km/h, and Figure 30 shows the overlap of the accelerations measured and calculated at speed *V2* = 117 km/h.

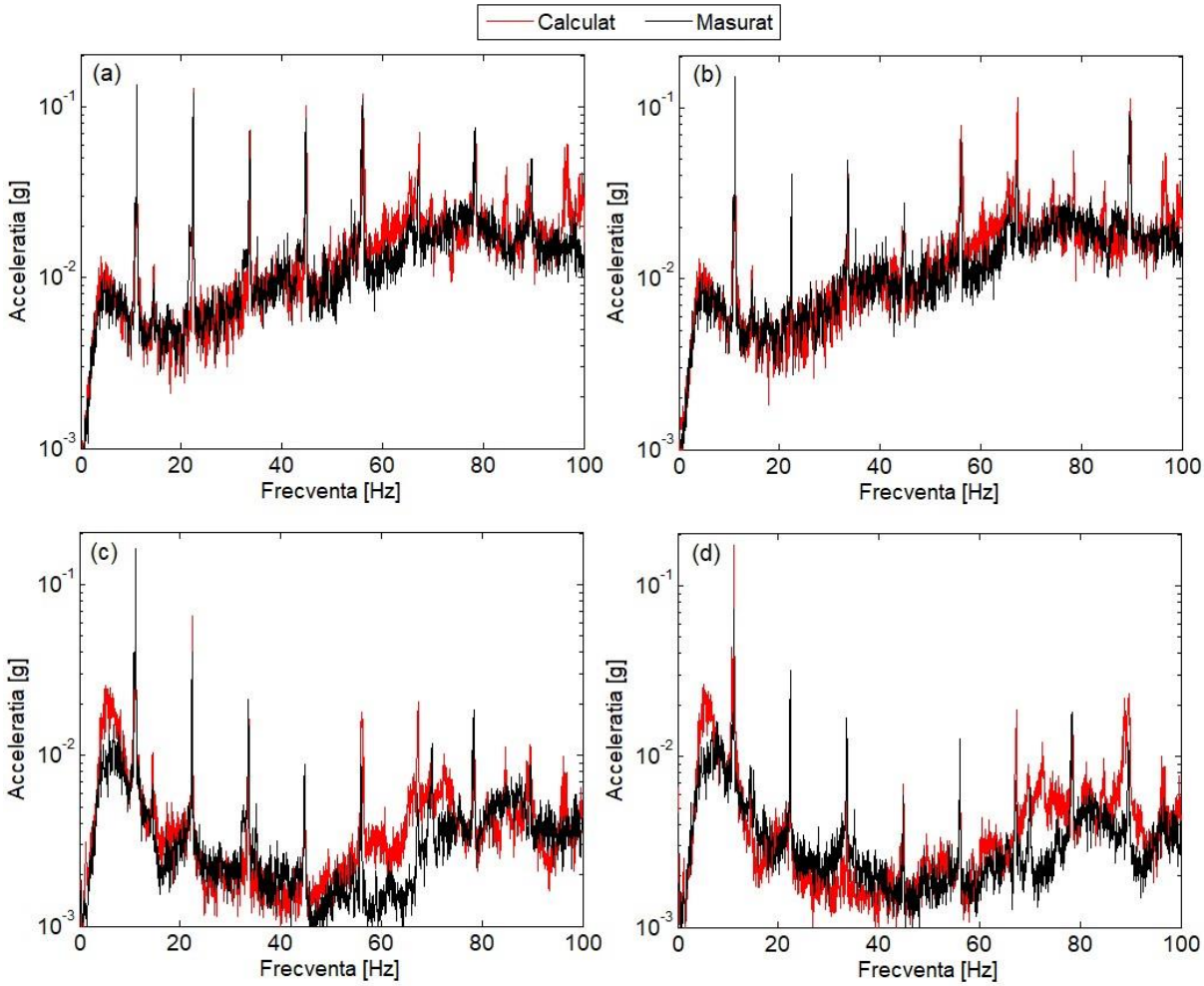


Fig. 30. Effective acceleration spectra calculated and measured at 117 km/h: (a) axle 1; (b) axle 2; (c) bogie frame above axle 1; (d) the bogie frame above axle 2.

In general, there is a good concordance between the two types of effective acceleration spectra, the one measured and the one calculated on the basis of the model presented in the work. At the level of axle boxes, the proximity between accelerations due to roughness of the treads is remarkable, which can be explained by the mediation procedure of the average quadratic acceleration measured on 12 track sections. At the level of the bogie frame, some differences between the measured and calculated accelerations can be signaled, but this is less important given the simplicity of the model chosen for the bogie.

Much more important are the observations that can be made in connection with the tips due to defects in eccentricity, ovality and polygonalization of the wheel. Not only do the frequencies of these peaks practically coincide, but the amplitudes obtained on the basis of the wheel-rail system model are close to those calculated at the level of the axle boxes.

In conclusion, the experimental and theoretical results validate the model of the rail wheel system proposed in this paper.

Thesis conclusions and personal contributions

The vibrations of the wheel-rail system are generated by the roughness of the treads, their quasi-periodic or local defects and the discontinuities of the running surface of the rail.

Regarding the vibration size of the wheel-rail system, a very important role is played by the rail pads, which represent the closest elastic element to the area where these vibrations are generated, and the prism of the path. The elastic characteristics of the rail plates and that of the porch of the path, representing the contact force corresponding to a sleeper end depending on the deformation, are nonlinear, and this aspect represents an important difficulty in solving the equations of motion of the path model.

It has been demonstrated that both the elastic characteristic of the rail plate and the elastic characteristic of the path prism can be approximated by linear force-displacement functions on bilinear portions. These functions shall be constructed by the method of the smallest squares according to the size of the static wheel load, so that the errors in relation to the non-linear characteristic are of the order of a few percent for the usual wheel loads in current vehicles.

The nonlinear characteristics of the rail pads and the ballast prism can be implemented in the model of the two-storey elastic path by using bilinear functions. The result is a nonlinear pattern of the railway whose equivalent elastic characteristic has three branches, on each of them the stiffness is constant.

It has been shown that the errors introduced in the route model as a whole by the bilinear characteristics of the rail plates and of the path prism in relation to the actual characteristics are less than the errors which appear in the calculation of the bilinear characteristics of the two elastic floors in relation to the actual elastic characteristics of each elastic floor separately.

The use of this model in the study of wheel-rail vibrations can be made if it is taken into account that the wheel-rail contact force has two components, one is constant over time and is equal to the static wheel load of the vehicle, and the other is variable over time and represents the dynamic component of the contact force.

Under the static load, the rail works on the branch with the highest rigidity around the section where the static load acts, then on the medium rigidity branch and, at a distance from the static load section, on the elastic branch. The distances on which the rail works on each branch are calculated by solving a nonlinear algebraic system resulting from the boundary conditions of the model.

Once the configuration of the elastic foundation of the path pattern according to the static load is established, the dynamic response of the rail can be calculated in terms of receptance. This stage is possible by linearizing the path model with nonlinear elastic characteristic around the equilibrium position under the static load. A linearized model with non-homogeneous elastic characteristic (MLCEN) was obtained. For comparison, an equivalent linear model with homogeneous elastic characteristic (MLCEO) has also been developed.

Regarding the analysis of the dynamic response of the rail, it is of interest to two aspects and certain: the response of the rail next to the active section (where the excitation force acts) for the influence it has on the vibration mode of the wheel-rail system and the way in which the bending waves along the rail are attenuated for the influence on the sound power of the rail.

The dynamic response of the rail on the foundation with homogeneous elastic characteristic (MLCEO) under the action of a harmonic force presents two resonance frequencies, one low at which the rail and sleepers vibrate in phase on the ballast prism and another, high at which the rail and sleepers vibrate in antiphase. Between the two resonances, the rail experiences the anti-resonance mode due to the dynamic absorbing effect exerted by the sleepers. Through the rail, two evanescent waves are propagated, which by composition form stationary waves at frequencies lower than the first resonant frequency and at frequencies between the frequency of anti-resonance and the second frequency of resonance. In the other two frequency ranges, between the first resonant frequency and the anti-resonance frequency, and at frequencies higher than the frequency of the second resonance, an evanescent wave propagates through the rail whose effect disappears near the excitation force and a propagation wave.

The cushioning of the rail pads and the crushed stone prism, whether shaped with the viscoelastic pattern or with the hysteretic pattern, limits the amplitude of the vibration to the resonant frequencies and reduces it in the areas around these frequencies. At the same time, damping increases the response of the rail around the anti-resonance frequency. The damping of the rail pads controls the amplitude of the rail around the high frequency of resonance, and the damping of the crushed stone prism controls the vibration mode of the rail around the low resonant frequency. Damping has no effects at high frequencies. At low frequencies, hysteretic damping reduces the amplitude of the response, while viscoelastic damping does not influence the dynamic mode because the latter being proportional to the frequency, at low frequencies the weight of the damping force becomes insignificant compared to that of the elastic force.

Regarding the attenuation of bending waves along the rail, both damping models indicate that the highest attenuation values are recorded in the frequency ranges where only evanescent waves are propagated through the rail. The hysteretic damping model shows that bending waves attenuate to a lesser extent in the range of frequencies greater than the high resonance frequency.

The dynamic rail response calculated with the linearized model with non-homogeneous elastic characteristic (MLCEN) is different from that obtained with MLCEO in the field of low and medium frequencies, but is similar in the high frequency range where the response no longer depends practically on the elasticity of the path, but on the inertia of the rail and sleepers. Low resonance frequency and anti-resonance frequency are higher if calculated with MLCEN. In addition, a series of maximums and lows appear in the receptance diagram located between the low resonance frequency and the anti-resonance frequency that did not correspond in the results obtained with MLCEO. The explanation of the differences between the results obtained with the two models lies, on the one hand, in the fact that the two models have different rigidities in the section where the harmonic excitation force acts, which makes the receptance is calculated with MLCEN closer to that calculated with a homogeneous foundation model that works but only on the rigid portions of the bilinear characteristics (rigid-rigid case), and on the other hand, in the appearance of stationary waves as a result of the waves reflected by the sections in which the MLCEN changes its rigidity.

In the case of using MLCEO, the same type of waves propagates through the rail over its entire length regardless of their frequency, if the frequency is within one of the 4 intervals delimited by the resonance and anti-resonance frequencies. The way in which bending waves propagate along the rail is different when MLCEN is applied in the sense that the nature of the waves can change at a small change in frequency, without the frequency passing from one interval to another from those delimited by the two resonances and anti-resonances. The change in the nature of the bending waves occurs when passing through the section where the change

in the rigidity of the foundation takes place. As a result, there is a notable difference between how the amplitude of the vibration along the rail determined decreases with those models.

The vibrational mode of the mounted axle, which has been studied in a robust manner using two different methods, the analytical method based on the euler-bernoulli beam theory for the axle with rigid bodies attached to the wheels and axle boxes and the finished element method, is dominated by the inertial character due to the rigid mode of vibration and the resonances of the axle induced by its bending. The bending vibration of the mounted axle has its own symmetrical and antisymmetric modes, respectively, which can be highlighted by symmetrical or antisymmetric modes of excitation. The proper frequencies of the antisymmetric modes are greater than the proper frequencies of the corresponding symmetric modes. Depending on the type of excitation, the mounted axle has anti-resonance modes at the level of the wheels and axle boxes at frequencies close to the resonant frequencies.

The vibrations of the wheel-rail system were studied using an original model comprising the pattern of the path, the mounted axle and the suspended mass of the bogie, also including the elements of the primary suspension. The vibration analysis was performed by the comparison method considering the two track models, the linearized model with non-homogeneous elastic characteristic and the linear model with homogeneous elastic characteristic, and two damping models, the viscous depreciation model and the hysteretic damping model. The harmonic vibration mode based on the frequency response and random vibration functions have been studied, calculating the power density spectra of the interest quantities and the spectra of effective values.

The calculations carried out using the MLCEO reveal the existence of three resonances of the system under analysis. The first resonant frequency is due to the suspended mass of the bogie and the primary suspension, and the other two, occurring at much higher frequencies, are due to the interaction between the axle and the railway. These resonances occur only in the frequency areas where stationary evanescent waves propagate through the rail.

The analysis of the frequency response function of the contact force results in the following correlations: the dynamic contact force becomes minimal at the resonance frequencies of the rail and in the vicinity of the wheel's anti-resonance frequencies. In addition, the wheel-rail contact force is minimal and at the resonant frequency of the system composed of the wheel-primary suspension-suspended mass of the bogie considered as a system with two degrees of freedom and an elastic degree of freedom.

Damping, regardless of the damping model adopted, limits the vibration amplitude to the resonance frequencies of the wheel-rail system, but amplifies it to the anti-resonance frequencies. Even if it takes relatively low values, damping can blur in some situations the existence of resonance and anti-resonance either at the wheel or axle box level, or at the level of the rail.

When using the hysteretic damping model, the maximums corresponding to the amplitude resonance appear at higher frequencies than those obtained with the viscous damping pattern.

Analysis of the spectral power densities of the acceleration shows that the forced vibration mode is dominated at low frequency by the vibration of the suspended mass of the bogie due to the resonance of amplitude. At frequencies ranging from the resonant frequency of the suspended mass on the primary suspension to the low resonant frequency of the axle on the track, the highest acceleration is recorded at wheel level so that at higher frequencies the rail becomes the most important source of vibration. In general, the acceleration of the rail increases with the frequency, except for the two areas around the resonant frequency of the axle

on the track when the acceleration of the rail shows local minimums. At the low resonant frequency of the axle on the track, the wheel and rail at the point of contact with the wheel have substantially equal vibrations.

Regarding the calculated forces, the force in the suspension and the contact force wheel-rail, it is noted that the contact force wheel-rail is higher over almost the entire frequency range.

As regards the differences between the results obtained with MLCEN and those obtained with MLCEO, the analysis shows that these differences are not influenced by the depreciation model adopted. Thus, the acceleration of the rail at the point of contact calculated with MLCEO is higher than that obtained with the help of MLCEN over almost the entire frequency range considered. The acceleration of the wheel shows frequency ranges in which the values given by MLCEO are higher than those resulting from MLCEN so that in others, the ratio between the values obtained with the two models is reversed.

Large differences can be reported between the results provided by the two models in terms of wheel-rail contact force. The differences are not only quantitative although they can take values from simple to double, but also qualitative, in the sense that while the spectral density calculated with one model has a local maximum, the spectral density calculated with the other model has a local minimum.

The parametric study of the vibrations of the wheel-rail system carried out using the linearized model with non-homogeneous elastic characteristic reveals the following aspects regarding the spectra of the effective values calculated on intervals of 1/3 octave.

Influence of the speed of movement:

(a) the acceleration of the wheel, the acceleration of the rail in the contact section with the wheel and the contact force monotonously increase depending on the speed of movement;

(b) with the increase in running speed, the distortion of the wheel acceleration spectra and the contact force in certain frequency bands occurs by changing the ratio of the spectral components with the increase in the running speed; Influence of static load:

(a) at a frequency lower than the low resonant frequency of the track axle, the acceleration of the rail decreases if the static load increases so that at high frequencies the acceleration of the rail is higher in some frequency ranges and lower in others;

(b) the acceleration of the wheel and the contact force are not influenced by static load at low frequencies, but at medium and high frequencies, they can show very large increases in certain intervals of 1/3 octave;

Influence of the elastic constant of the *rigid* portion of the rail plate characteristic:

(a) the increase in stiffness leads to a reduction in the vibration of the rail over almost the entire frequency range, except for one to two frequency ranges in which the increase is modest;

(b) the increase in rigidity does not influence the vibration of the wheel and the contact force in the field of low and high frequencies, but it does cause a sharp increase in the field of average frequencies.

Influence of the elastic constant of the *elastic* portion of the rail plate characteristic:

(a) the increase in stiffness reduces the vibration of the rail in the low frequency range and has a limited influence in the rest either by lowering the level of vibration or by increasing it in certain frequency ranges;

(b) increased rigidity can lead to an appreciable amplification of the vibration of the wheel and of the contact force within a certain frequency range, but otherwise it either does not practically

influence the vibration mode, or this influence is modest. The conclusions of the parametric study can be applied in all practical problems of the vibrations of the wheel-rail system contributing to the better knowledge of the interaction phenomena, especially of those phenomena related to the production of rolling noise and the initiation and development of tread wear.

At the same time, the vibration model of the wheel-rail system and the conclusions of the parametric study can be a guide for finding the best solution regarding the design of the rail pads according to the main parameters of the roadway and the characteristics of the vehicles driving on a certain section of trackside.

Personal contributions

In this section are presented the most important contributions of the thesis.

(a) Methodology for determining the bilinear approximation of the force-deformation characteristic of the rail plates and the crushed stone prism according to the maximum load and the maximum permissible error;

(b) Implementation of the bilinear characteristics of the rail pads and the crushed stone porches in the nonlinear model of the railway consisting of an infinite Euler-Bernoulli beam on a foundation with two elastic layers and an inertial intermediate layer; elaboration of the linearized model with non-homogeneous elastic characteristic and elaboration of the linear model with homogeneous elastic characteristic which is used as a comparison term in assessing the vibration mode of the wheel-rail system.

(c) Elaboration of the method of solving the nonlinear equations describing the displacement of the rail and of the sleepers under the action of static load and the determination of the elastic constants of the elastic layers of the linear model with homogeneous elastic characteristic, provided that the displacement of the rail and the sleepers in the section of the static load is equal to those obtained with the nonlinear model;

(d) Deduction of the equations of the dynamic mode of the linearized model with non-homogeneous elastic characteristic and of the equations of the dynamic mode of the linear model with homogeneous elastic characteristic;

(e) Analysis of the dynamic response of the rail using the comparative method based on the results provided by MLCEN and MLCEO with the punctuation of the following more important aspects: the determination of the types of waves that propagate through the rail in accordance with the properties of the two models and the frequency ranges at which these waves occur; the highlighting of the stationary waves as a result of the reflection of the bending waves in the sections where the variation of the rigidity of the elastic layers of the foundation occurs; analysis of the track dynamic response obtained with MLCEN and MLCEO taking into account two models of depreciation, viscous depreciation and hysteretic damping and highlighting the differences that occur between the results due to the use of the two damping models; analysis of how the bending waves calculated with MLCEN and MLCEO propagate along the rail;

(f) The study of the vibration mode of the axle mounted with the help of two models, one analytical, based on the euler-bernoulli beam theory with rigid masses attached, and the other built on the theory of the finished element to verify the results obtained: the resonant frequency of the axle bending, the receptance of the axle next to the wheels and next to the axle boxes for the symmetrical and antisymmetric modes of vibration;

(g) Elaboration of the model for the study of the vibrations of the wheel-rail system based on the nonlinear model of the railway characterized by the modeling with bilinear functions of the rigidity of the elastic layers corresponding to the rail plates and the broken stone porches, of the model with finished elements of the mounted axle and with the inclusion of the suspended mass of the bogie and the effect of the primary suspension;

(h) Methodology for determining the spectral power density of the excitation factor of the wheel-rail system vibrations in analytical form based on the density spectrum of the quadratic mean of the leveling deviations given in analytical form and the limit spectrum in 1/3 octave bands of the rolling surface roughness required by the norms on the noise measurement conditions of railway vehicles;

(i) Parametric analysis of the wheel-rail vibrations based on the linearized model with non-homogeneous elastic characteristic that highlights the influence of the running speed, the static wheel load and the elastic constants of the 'elastic' and 'rigid' portion of the rail plate characteristic on the vibration mode;

(j) Method of validation of the theoretical model on the basis of experimental tests to measure acceleration at axle box level at different running speeds when the wheel-rail vibration excitation factor contains a deterministic component (wheel polygonalisation defect) and a random component (rolling surface roughness).

Directions for research development

Starting from the achievements presented in this paper, future research can develop in the following directions:

(a) Application of the nonlinear tread pattern consisting of a Euler-Bernoulli beam resting on a continuous foundation with two elastic layers with bilinear elastic characteristics for the rail plates and the crushed stone prism to study the vibration mode caused by the interaction between a two- or four-axle vehicle. A similar method may be used, namely the determination of the equilibrium position below the static load and then the calculation of the rail-level receptances in the sections of contact with the wheels of the vehicle;

(b) Application of the nonlinear railway model described in this paper to study the phenomena of vehicle/track interaction in the field of high traffic speeds by adopting the mobile wheel interaction model; in a first phase, the critical track speed, i.e. the phase velocity of the bending rail waves must be determined; studying the phenomena of instability of the vehicle-track system due to abnormal Doppler waves that can be induced in the structure of the vehicle traffic path;

(c) Extension of the frequency range in which it can be applied to the track model with bilinear characteristics for the ballast prism rail plates by replacing the continuous foundation with a foundation with equidistant point supports; solving the problem of the interaction between the vehicle and the track can be done by adopting a finite-length track model and solving the equations of motion by applying the method of modal analysis. By applying this method, the path response is described by a system of differential equations with ordinary nonlinear derivatives coupled due to the presence of nonlinear terms in the expression of the forces in the supports, and solving such a system of equations can be done by applying the Newmark-beta method.

Bibliography

1. Ahmad, N., Thompson, D.J., Jones, C.J.C., Muhr, A.H., Predicting the effect of temperature on the performance of elastomer-based rail damping devices, Journal of Sound and Vibration 322 (2009) 674-689.
2. Arlaud, E., Costa D'Aguiar, S., Balmes, E., Receptance of railway tracks at low frequency: Numerical and experimental approaches, Transportation Geotechnics 9 (2016) 1-16.
3. Baeza, L., Fayos, J., Roda, A., Insa, R., High frequency railway vehicle-track dynamics through flexible rotating wheelsets, Vehicle System Dynamics 46 (2008) 647-662.
4. Baeza, L., Vila, P., Xie, G., Iwnicki, S., Prediction of rail corrugation using a rotating flexible wheelset coupled with a flexible track model and a non-Hertzian/non-steady contact model, Journal of Sound and Vibration 330 (2011) 4493–4507
5. Berggren, E., Railway Track Stiffness Dynamic Measurements and Evaluation for Efficient Maintenance, PhD thesis, ISSN 1651-7660 ISBN 978-91-7415-293-7, Royal Institute of Technology (KTH), Stockholm, 2009.
6. Bezin, Y., Farrington, D., Penny, C., Temple, B., Iwnicki, S., The dynamic response of slab track constructions and their benefit with respect to conventional ballasted track, Vehicle System Dynamics 48 Supplement (2010) 175-193.
7. Bracciali, A., Cascini, G., Ciuffi, R., Time Domain Model of the Vertical Dynamics of a Railway Track up to 5 kHz, Vehicle System Dynamics 30 (1998) 1-15.
8. Horses, Z., Raymond, G. P., Bathurst, R. J., Estimate of Static Track Modulus using elastic foundation models, Transportation Research Record 1470, 1994, 65-72.
9. Carrascal, I.A., Casado, J.A., Polanco, J.A., Gutierrez-Solana, F. Dynamic behaviour of railway fastening setting pads, Engineering Failure Analysis 14 (2007) 364-373.
10. Carrascal, I.A., Perez, A., Casado, J.A., Diego, S., Polanco, J.A., Ferreno, D., Martin, J. J., Experimental study of metal cushion pads for high speed railways, Construction and Building Materials 182 (2018) 273-283.
11. Castro Jorge, P.C., Pinto da Costa, A., Simões, F.M.F., Finite element dynamic analysis of finite beams on a bilinear foundation under a moving load, Journal of Sound and Vibration 346 (2015) 328-344.
12. Chandra, S., Agarwal, M.M., Railway engineering, Oxford University Press 2007, New Delhi.
13. Chen, Y.Z., He, C.G., Zhao, X.J., Shi, L.B., Liu, Q.Y., Wang, W.J., The influence of wheel flats formed from different braking conditions on rolling contact fatigue of railway wheel, Engineering Failure Analysis 93 (2018) 183-199.
14. Cheng, G., He, Y., Han, J., Sheng, X., Thompson, D., An investigation into the effect of modelling assumptions on sound power radiated from a high-speed train wheelset, Journal of Sound and Vibration 495 (2021) 115910.
15. Connolly, D. P., Kouroussis, G., Woodward, P. K., Alves Costa, P., Verlinden, O., Forde, M.C., Field testing and analysis of high speed rail vibrations, Soil Dynamics and Earthquake Engineering 67 (2014) 102-118.
16. Connolly, D. P., Kouroussis, G., Laghrouche, O., Ho, C. L., Forde, M.C., Benchmarking railway vibrations – Track, vehicle, ground and building effects, Construction and Building Materials 92 (2015) 64-81.

17. Connolly, D. P., Marecki, G. P., Kouroussis, G., Thalassinakis, I., Woodward, P. K., The growth of railway vibration ground problems — A review, Science of the Total Environment 568 (2016) 1276-1282.

18. Correa, N., Vadillo, E., Santamaria, J., Blanco-Lorenzo, J., On the non-proportionality between wheel/rail contact forces and speed during wheelset passage over specific weld, Journal of Sound and Vibartion 413 (2018) 79-100.

19. Cruceanu, I.C., Sorohan, Ș., Determination of the harmonic response of a railway wheelset using the finite element analysis method, The 13th International Conference

Interdisciplinarity in Engineering, 3 – 4 October 2019, Tirgu Mures, Romania, published in Procedia Manufacturing, Vol. 46, 2020, pp. 173-179.

20. Dimitrovová, Z., Frýba, L., Transverse Vibrations in Beams Supported by a Piece-Wise Homogeneous Visco-Elastic Foundation, Proceedings of the Twelfth International Conference on Civil, Structural and Environmental Engineering Computing", Civil-Comp Press, Stirlingshire, UK, Paper 44, 2009.

21. Dimitrovova, Z., Critical velocity of a load moving on a beam with a sudden change of foundation stiffness: Applications to high-speed trains, Computers and Structures 87 (2009) 1224-1232.

22. Dimitrovova, Z., A general procedure for the dynamic analysis of finite and infinite beams on piece-wise homogeneous foundation under moving loads, Journal of Sound and Vibration 329 (2010) 2635-2653.

23. Dimitrovova, Z., Rodrigues, A.F.S., Critical velocity of a uniformly moving load, Advances in Engineering Software 50 (2012) 44-56.

24. Ding, H., Shi, K-L., Chen, L-Q., Yang, S-P. Dynamic response of an infinite Timoshenko beam on a nonlinear viscoelastic foundation to a moving load, Nonlinear Dynamics 73 (2013) 285-298.

25. Dings, P.C., Dittrich, M.G. Roughness on Dutch railway wheels and rails, Journal of Sound and Vibration 193 (1996) 103-112.

26. Dossing, O., Structural Testing, Bruel&Kjaer, Nærum 1988.

27. Dumitriu, M., Cruceanu, I.C., On the rolling noise reduction by using the rail damper, Journal of Engineering Science and Technology Review, Vol. 10, Issue 6, 2017, pp. 87-95.

28. Dumitriu, M., Cruceanu, I.C., Methods and techniques for reducing the noise emitted by the rail, National Symposium of Railway Rolling Stock - XV-th edition – Bucharest 2017, MatrixRom Publishing House, pag. 161-185, ISSN 1843-9888.

29. Dumitriu, M., Gheţi, M.A., Cruceanu, I.C., Experimental analysis of the vertical vibration of the railway bogie during braking, The 13th International Conference Interdisciplinarity

in Engineering, 3 – 4 October 2019, Tirgu Mures, Romania, published in Procedia Manufacturing, Vol. 46, (2020) 49-54.

30. Dumitriu, M., Cruceanu, I.C., Effect of vertical track irregularities on the vibration of railway bogie, UPB Scientific Bulletin, Series D: Mechanical Engineering, Vol. 81, Issue 1, 2019, pp. 67-78.

31. Dumitriu, M., Cruceanu, I.C., Analysis of the vertical vibrations of the Minden-Deutz bogie based on experimental data, National Symposium of Railway Rolling Stock - XVII-th edition – Bucharest 2019, MatrixRom Publishing House, ISSN 1843-9888, pag. 98-107.

32. Dumitriu, M., Cruceanu, I.C., Fologea, D., Experimental study of the bogie vertical vibration - correlation between bogie frame accelerations and wheelsets accelerations, UPB Scientific Bulletin, Series D: Mechanical Engineering, Vol. 83, Issue 2, 2021, pp. 83-94.

33. Dumitriu, M., Fologea, D., Cruceanu, I.C., Effects analysis of vertical track irregularities on bogie vibration - method based on bogie modelling and wheelsets accelerations measurement, 11th International Conference on Advanced Manufacturing Technologies

(ICAMaT 2020), October 29 - 30, 2020, Bucharest, Romania, published in IOP Conf. Series: Materials Science and Engineering, Vol. 1018, 2021, Article number 012001, 9 pages.

34. Dumitriu, M., Mazilu, T., Vibrations. Numerical and experimental applications, Matrix Rom Publishing House, Bucharest, 2012.

35. Egana, J.I., Vinolas, J., Seco, M., Investigation of the influence of rail pad stiffness on rail corrugation on a transit system, Wear 261 (2006) 216-224.

36. Ebersohn, W., Selig, E., Track Modulus Measurements on a Heavy Haul Line, Transportation Research Record 1470, 1994, 73-83.

37. Elias, J., Simulation of railway ballast using crushable polyhedral particles, Powder Technology, 264 (2014) 458-465.

38. El-sayed, H.M., Zohny, H. N., Riad, H. S., Fayed, M. N., A three-dimensional finite element analysis of concrete sleepers and fastening systems subjected to coupling vertical and lateral loads, Engineering Failure Analysis 122 (2021) 105236.

39. Esveld, C., Modern Railway Track, Second Edition, TU Delft, MRT, 2001.

40. Fermer, M., Nielsen, J.C. O., Wheel/Rail Contact Forces for Flexible versus Solid Wheels due to Tread Irregularities, Vehicle System Dynamics 23 (1994) 142-157.

41. Ferreno, D., Sainz-Aja, J., Carrascal, I, Cuartas, M., Pombo, J., Casado, J., Diego, S., Prediction of mechanical properties of rail pads under in-service conditions through machine learning algorithms, Advances in Engineering Software 151 (2021) 102927.

42. Froio, D., Rizzi, E., Simões, F.M. F., Pinto da Costa, A., Dynamics of a beam on bilinear elastic foundation under harmonic moving load, Acta Mechanica 229 (2018) 4141–4165.

43. Froio, D., Structural dynamics modelization of one-dimensional elements on elastic foundations under fast moving load, Universita degli Studi di Bergamo, 2020.

44. Froling, R. D., Scheffel, H., Ebersohn, W., The vertical dynamic response of a rail vehicle caused by track stiffness variation along the track, Vehicle System Dynamics Supplement 25 (1996) 175-187.

45. Ge, X., Ling, L., Yuan, X., Wang, K., Effect of distributed support of rail pad on vertical vehicle-track, Construction and Building Materials 262 (2020) 120607.

46. Grassie, S. L., Gregory R. W., Harrison D., Johnson, K.L. The dynamic response of railway track to high frequency vertical excitation, *Journal Mechanical Engineering Science* 24 (1982) 77-90.

47. Gu, G., Choi, J., The dynamic response of rail support, Vehicle System Dynamics 51 (6) (2013) 798-820.

48. Guo, Y., Jia, W., Markine, V., Guoqing Jing, G., Rheology study of ballast-sleeper interaction with particle image velocimetry (PIV) and discrete element modelling (DEM), Construction and Building Materials 282 (2021) 122710.

49. Hasan, N., Rail Pad Stiffness and Classification System, Journal of Transportation Engineering, Part A: Systems 145 (2019) 04019012.

50. Hila, V., Radu, C., Ungureanu, C., Stoicescu, G., Railways Part I Basics of Railway Design, Institute of Constructions, Bucharest 1975.

51. Hila, V., Radu, C., Ungureanu, C., Stoicescu, G., Căi ferate Parte II Suprastructura caleii, Institutul de Construcții, Bucureşti 1975.

52. Hussein, M.F.M., Hunt, H. E.M., Modelling of floating-slab tracks with continuous slabs under oscillating moving loads, Journal of Sound and Vibration 297 (2006) 37-54.

53. Iwnicki, S., Spiryagin, M., Cole, C., McSweeney, T., Handbook of Railway Vehicle Dynamics, Second edition, 2020, CRC Press, Taylor& Francis Group.

54. Jin, H., Zhou, X., Sun, X., Li, Z., Decay rate of rail with egg fastening system using tuned rail damper, Applied Acoustincs 172 (2021) 107622.

55. Johnson, K.L., Contact Mechanics. Cambridge University Press, Cambridge, 1985.

56. Jones, C. J.C., Thompson, D. J., Diehl, R. J., The use of decay rates to analyse the performance of railway track in rolling noise generation, Journal of Sound and Vibration 293 (2006) 485-495.

57. Kaewunruen, S., Remennikov, A.M., Integrated field measurements and track simulations for condition assessment of railway tracks, 1st International Conference on Structural Condition Assessment, Monitoring, and Improvement, Perth, Australia, December 12-14, 2005, 391-398.

58. Kaewunruen, S., Remennikov, A.M., Sensitivity analysis of free vibration characteristics of an in-situ railway concrete sleeper to variations of rail pad parameters, Journal of Sound and Vibration 298 (2006) 453-461.

59. Kaewunruen, S., Remennikov, A., Field trials for dynamic characteristics of railway track and its components using impact excitation technique, NDT&E International 40 (2007) 510519.

60. Kaewunruen, S., Remennikov, A.M., An Alternative Rail Pad Tester for Measuring Dynamic Properties of Rail Pads Under Large Preloads, Experimental Mechanics 48 (2008) 55-64.

61. Kaewunruen, S., Remennikov, A., Dynamic properties of railway track and its components : a state-of-the-art review, Weiss, BN (ed) New Research on Acoustics, Hauppauge, New York, Nova Science Publishers, 2008, 197-220.

62. Kaiser, I., Popp, K., Interaction of elastic wheelsets and elastic rails: modelling and simulation, Vehicle System Dynamics 44 Supplement (2006) 932-939.

63. Knothe, K., Wu, Y. Receptance behaviour of railway track and subgrade, Archive of Applied Mechanics 68 (1998) 457- 470.

64. Koroma, S., Hussein, M., Owen, J., Influence of Preload and Nonlinearity of Railpads on Vibration of Railway Tracks under Stationary and Moving Harmonic Loads, Journal of Low Frequency Noise, Vibration and Active Control 34/3 (2015) 289-306.

65. Koroma, S., Hussein, M., Owen, J., The effects of preload and nonlinearity on the vibration of railway tracks under harmonic load, 11th International Conference on Vibration Problems Lisabon, Portugal 9-12 Sept 2013.

66. Kouroussis, G., Connolly, D. P., Verlinden, O., Railway-induced ground vibrations – a review of vehicle effects, International Journal of Rail Transportation 2 (2014) 69-110.

67. Kostovasilis, D., Thompson, D. J., Hussein, M.F.M., A semi-analytical beam model for the vibration of railway tracks, Journal of Sound and Vibration 393 (2017) 321-337.

68. Lei, X., High Speed Railway Track Dynamics – Models, Algorithms and Applications, Springer 2017 (ISBN 978-981-10-2039-1).

69. Li, W., Dwight, R., Zhang, T., On the study of vibration of a supported railway rail using the semi-analytical finite element method, Journal of Sound and Vibration 345 (2015) 121145.

70. Li, L., Thompson, D. J., Xie, Y., Zhu, Q., Luo, Y., Lei, Z., Influence of rail fastener stiffness on railway vehicle interior noise, Applied Acoustics 145 (2019) 69-81.

71. Luo, Y., Liu, Y., Yin, H. P., Numerical investigation of nonlinear properties of a rubber absorber in rail fastening systems, International Journal of Mechanical Sciences 69 (2013) 107-113.

72. Maes, J., Sol, H., Guillaume, P., Measurements of the dynamic railpad properties, Journal of Sound and Vibration 293 (2006) 557-565.

73. Maglio, M., Pieringer A., Nielsen, J.C. O., Vernersson, T., Wheel–rail impact loads and axle bending stress simulated for generic distributions and shapes of discrete wheel tread damage, Journal of Sound and Vibration 502 (2021) 116085.

74. Martínez-Casas, J., Giner-Navarro, J., Baeza, L., Denia, F.D., Improved railway wheelset–track interaction model in the high-frequency domain, Journal of Computational and Applied Mathematics 309 (2017) 642–653.

75. Mazilu, T., Green's functions for analysis of dynamic response of wheel/rail to vertical excitation, Journal of Sound and Vibration 306 (2007) 31-58.

76. Mazilu, T., Vibrații roată-rail, Matrixrom, Bucharest, 2008.

77. Mazilu, T., Vibrații, Matrixrom, Bucharest, 2012.

78. Mazilu, T. The dynamics of an infinite uniform Euler-Bernoulli beam on bilinear viscoelastic foundation under moving loads, Procedia Engineering 199 (2017) 2561-2556 – X International Conference on Structural Dynamics, EURODYN 2017.

79. Mazilu, T., Interaction between moving tandem wheels and an infinite rail with periodic supports - Green's matrices of the track method in stationary reference frame, *Journal of Sound and Vibration* 401 (2017) 233-254.

80. Mazilu, T., Dumitriu, M., Tudorache, C., Sebeșan, M., Using the Green's functions method to study wheelset/ballasted track vertical interaction, Mathematical and Computer Modelling 54 (2011) 261-279.

81. Mazilu, T., Cruceanu, I.C., Techniques for measuring noise in railway vehicles, Railway Rolling Stock Symposium - XIV-th edition, Bucharest, 2016, Matrix Rom Publishing House, ISSN 1843-9888, pag. 116 - 125.

82. Mazilu, T., Cruceanu, I.C., Dynamics of a beam on elastic foundation – impact of the bilinear characteristic of the foundation upon the propagation of the bending wave, MATEC Web of Conferences - 22st Innovative Manufacturing Engineering & Energy International

    Conference – IManE&E 2018, Chisinau, Republic of Moldova, May 31 - June 2, 2018, Vol. 178, 2018, Article number 06008.

83. Mazilu, T., Cruceanu, I.C., Numerical study of the interaction between a moving oscillator and an infinite beam on elastic foundation with bilinear characteristic, IOP Conf. Series: Materials Science and Engineering, The 8th International Conference on Advanced Concepts in

Mechanical Engineering - ACME 2018, 13 – 16 June 2018, Vol. 444, 2018, number Article 042004.

84. Mazilu, T., Dumitriu, M., Tudorache, C., Instability of an oscillator moving along a Timoshenko beam on viscoelastic foundation, Nonlinear Dynamics 67 (2012) 1273-1293.

85. Mortensen, J., Faurholt, J. F., Hovad, E., Walther, J. H., Discrete element modelling of track ballast capturing the true shape of ballast stones, Powder Technology 386 (2021) 144-153.

86. Morys, B. Enlargement of out of round wheel profiles on high speed trains, Journal of Sound and Vibration 227 (1999) 965-978.

87. Nguyen, T. P., Pham, D. T., Hoang, P. H., A New Foundation Model for Dynamic Analysis of Beams on Nonlinear Foundation Subjected to a Moving Mass, Procedia Engineering 142 (2016) 166-173.

88. Ngamkhanong, C., Kaewunruen, S., Effects of under sleeper pads on dynamic responses of railway prestressed concrete sleepers subjected to high intensity impact loads, Engineering Structures 214 (2020) 110604.

89. Nielsen, J.C.O., High-frequency vertical wheel–rail contact forces—Validation of a prediction model by field testing, Wear 265 (2008) 1465–1471.

90. Oregui, M., Li, Z., Dollevoet, R., An investigation into the modeling of railway fastening, International Journal of Mechanical Sciences 92 (2015) 1-11.

91. Oregui, M., Li, Z., Dollevoet, R., Identification of characteristic frequencies of damaged railway tracks using field hammer test measurements, Mechanical Systems and Signal Processing 54-55 (2015) 224-242.

92. Oregui, M., Li, Z., Dollevoet, R., An investigation into the vertical dynamics of tracks with mono block sleepers with a 3D finite-element model, Proceedings of the Institution of Mechanical Engineers, Part F: Journal of Rail and Rapid Transit 230 (2015) 891-908.

93. Oregui, M., de Man, A., Woldekidan, M.F., Li, Z., Dollevoet, R., Obtaining railpad properties via dynamic mechanical analysis, Journal of Sound and Vibration 363 (2016) 460-472.

94. Ouyang, H., Moving-load dynamic problems: A tutorial (with a brief overview), Mechanical Systems and Signal Processing 25 (2011) 2039-2060.

95. Pfaffinger, M., Higher Vibration Modes in Railway Tracks at their Cutoff, Swiss Federal Institute of Technology, Zurich 2000.

96. Pieringer, A., Kropp, W., Nielsen, J.C. O., The influence of contact modelling on simulated wheel/rail interaction due to wheel flats, Wear 314 (2014) 273-281.

97. Ping Wang, Qiang Yi, Caiyou Zhao, Mengting Xing, Jian Tang, Wave propagation in periodic track structures: band-gap behaviours and formation mechanisms, Archive of Applied Mechanics 87 (2017) 503–519.

98. Radeş, M., Finite Element Analysis, Ed. Printech, Bucharest, 2006.

99. Read, D., Chrismer, S., Ebersohn, W., Selig, E., Track Modulus Measurements at the Pueblo Soft Subgrade Site, Transportation Research Record: Journal of the Transportation Research Board 1470 (1994) 55-64.

100. Remennikov, A., Kaewunrue, S., Determination of dynamic properties of rail pads using an instrumented hammer impact technique, Acoustics Australia 33 (2005) 63-67.

101. Remennikov, A., Kaewunruen, S., Laboratory measurements of dynamic properties of rail pads under incremental preload, 19th Australasian Conference on the Mechanics of Structures and Materials, Nov 29 - Dec 1, 2007, Christchurch, New Zealand, 319-324, Taylor & Francis.

102. Ryue, J., Thompson, D.J., White, P.R., Thompson, D. R., Investigations of propagating wave types in railway tracks at high frequencies, Journal of Sound and Vibration 315 (2008) 157-175.

103. Ryue, J., Thompson, D.J., White, P.R., Thompson, D. R., Decay rates of propagating waves in railway tracks at high frequencies, Journal of Sound and Vibration 320 (2009) 955-976.

104. Sainz-Aja, J., Carrascal, I, Ferreno, Pombo, J., Casado, J., Diego, S. Influence of the operational conditions on static and dynamic stiffness of rail pads, Mechanics of Materials 148 (2020) 103505.

105. Sato, Y., Morimura, T., Watanabe, S., Theoretical Analyses and Experimental Results on Track Moduli with Use of Wheelset Drop Test, Vehicle System Dynamics Suppleent 24 (1995) 164-179.

106. Sayeed, M. A., Shahin, M. A., Three-dimensional numerical modelling of ballasted railway track foundations for high-speed trains with special reference to critical speed, Transportation Geotechnics 6 (2016) 55-65.

107. Sebeşan, I., Mazilu, T., Vibrațiile vehiculelor feroviar, Matrixrom, 2010, Bucharest.

108. Selig, E., Li, D., Track Modulus: Its Meaning and Factors Influencing It, Transportation Research Record: Journal of the Transportation Research Board 1470 (1994) 47-54.

109. Shen, C., Deng, X., Wei, Z., Dollevoet, R., Zoetemand, A., Li, Z., Comparisons between beam and continuum models for modelling wheel-rail impact at a singular rail surface defect, International Journal of Mechanical Sciences 198 (2021) 106400.

110. Sheng, X., Jones, C.J.C., Thompson, D.J., Responses of infinite periodic structures to moving or stationary harmonic loads, Journal of Sound and Vibration 282 (2005) 125-149.

111. Sheng X., Thompson, D.J., Jones, C.J.C., Xie, G., Iwnicki, S.D., Allen, P., Hsu, S.S., Simulations of roughness initiation and growth on railway rails, Journal of Sound and Vibration 293 (2006) 819-829.

112. Shi, G., Wang, K., Huang, Q., Zhang, X., Influences of Stiffness of Rail Pads on System Dynamic Performances of Heavy Haul Railway, in Intelligent Computing, Networked Control, and Their Engineering Applications Volume 762 ed. Dong, Y., Chen, P., Dajun, D., Zhang, Tengfei, Z., Z., Z., Han, Qinglong, H., (2017) 618–628 Springer Nature Singapore Pte Ltd. 2017.

113. Shi, X., Liu, Y., Liu, Z., Hoh, H. J., Tsang, K. S., Pang, J. H. L., An integrated fatigue assessment approach of rail welds using dynamic 3D FE simulation and foreign monitoring technique, Engineering Failure Analysis 120 (2021) 105080.

114. Sol-Sanchez, M., Moreno-Navarro, F., Rubio-Gamez, C., The use of deconstructed tire rail pads in railroad tracks: Impact of pad thickness, Materials and Design, 58 (2014) 198-203.

115. Sol-Sanchez, M., Moreno-Navarro, F., Rubio-Gamez, C., Viability analysis of deconstructed tires as material for rail pads in high-speed railways, Materials and Design, 64 (2014) 407-414.

116. Sol-Sanchez, M., Moreno-Navarro, F., Rubio-Gamez, C., The use of elastic elements in railway tracks: A state of the art review, Construction and Building Materials 75 (2015) 293-305.

117. Sorohan, Ş., Constantinescu, I. N., Practica modelării şi analiza cu elemente finite, Ed. Printech, Bucureşti, 2003.

118. Squicciarini, G., Toward, M.G.R., Thompson, D.J., Experimental procedures for testing the performance of rail dampers, Journal of Sound and Vibration 359 (2015) 21-39.

119. Stoicescu, G., Suprastructura căii ferate, Conspress, Bucharest, 2009.

120. Szolc, T., Simulation of Bending-Torsional-Lateral Vibrations of the Railway WheelsetTrack System in the Medium Frequency Range, Vehicle System Dynamics 30 (1998) 473508.

121. Szolc, T., Simulation of Dynamic Interaction between the Railway Bogie and the Track in the Medium Frequency Range, Multibody System Dynamics 6 (2001) 99-122.

122. Thompson, D.J. Wheel/rail noise generation, Part II: wheel vibration, Journal of Sound and Vibration vol. 161, 1993, 401-419.

123. Thompson, D. J., A continuous damped vibration absorber to reduce broad-band wave propagation in beams, , Journal of Sound and Vibration 311 (2008) 824-842.

124. Thompson, D., Noise and Vibration Mechanisms Modelling and Means of Control, Ed. Elsevier, 2009, Linacre House, Jordon Hill, Oxford OX2 8DP, UK.

125. Thompson, D. J., Gautier, P-E, Review of research into wheel/rail rolling noise reduction, Proceedings of the Institution of Mechanical Engineers, Part F_ Journal of Rail and Rapid Transit 220 (2006) 385-408.

126. Thompson, D. J., Jones, C. J.C., Wu, T. X., de France, G. The influence of the non-linear stiffness behaviour of rail pads on the track component of rolling noise, Proceedings of the Institution of Mechanical Engineers, Part F: Journal of Rail and Rapid Transit 213 (1999) 233-241.

127. Thompson, D. J., van Vliet, W. J., Verheij, J. W., Developments of the indirect method for measuring the high frequency dynamic stiffness of resilient elements, Journal of Sound and Vibration 213 (1998) 169–188.

128. Thompson, D., Vincent, N., Track Dynamic Behaviour at High Frequencies. Part 1: Theoretical Models and Laboratory Measurements, Vehicle System Dynamics Supplement 24 (1995) 86-99.

129. Tran, M. T., Ang, K. K., Luong, V. H., Vertical dynamic response of non-uniform motion of high-speed rails, Journal of Sound and Vibration 333 (2014) 5427-5442.

130. Verheijen, E., A survey on roughness measurements, Journal of Sound and Vibration 293 (2006) 784-794.

131. Vincent, N., Thompson, D. J., Track Dynamic Behaviour at High Frequencies. Part 2: Experimental Results and Comparisons with Theory, Vehicle System Dynamics 24 (1995) 100-114.

132. Wang, P., Wang, L., Chen, R., Jinhui Xu, J., Xu, J. Gao, M., Overview and outlook on railway track stiffness measurement, Journal of Modern Transportation 24 (2016) 89-102.

133. Wei, K., Yang, Q., Dou, Y., Wang, F., Wang, P., Experimental investigation into temperature- and frequency-dependent dynamic properties of high-speed rail pads, Construction and Building Materials 151 (2017) 848-858.

134. With, C., Bordare, A., Evaluation of track stiffness with a vibrator for prediction of traininduced displacement on railway embankments, Soil Dynamics and Earthquake Engineering 29 (2009) 1187-1197.

135. Wu, T. X., On the railway track dynamics with rail vibration absorber for noise reduction, Journal of Sound and Vibration 309 (2008) 739-755.

136. Wu, T. X., Thompson, D.J., The effects of local preload on the foundation stiffness and vertical vibration of railway track, Journal of Sound and Vibration (1999) 219(5), 881–904.

137. Wu, T. X., Thompson, D.J., A Double Timoshenko Beam Model for Vertical Vibration Analysis of Railway Track at High Frequencies, Journal of Sound and Vibration 224 (1999) 329-348.

138. Wu, T. X., Thompson, D. J., Theoretical Investiagtion of Wheel/Rail Non-Linear Interaction due to Roughness Excitation, Vehicle System Dynamics 34 (2000) 261-282.

139. Wu, T. X., Thompson, D. J., Vibration analysis of railway track with multiple wheels on the rail, Journal of Sound and Vibration 239 (2001) 69-97.

140. Wu, T. X., Thompson, D.J., Behaviour of the Normal Contact Force Under Multiple Wheel/Rail Interaction, Vehicle System Dynamics 37 (2002) 1157-174.

141. Wu, T. X., Thompson, D. J., Wheel/Rail Non-linear Interactions With Coupling Between Vertical and Lateral Directions, Vehicle System Dynamics 41 (2004) 27-49.

142. Wu, T. X., Thompson, D. J., On the parametric excitation of the wheel/track system, Journal of Sound and Vibration 278 (2004) 725-747.

143. Wu, X., Rakhej, S., Cai, W., Chi, M., Ahmed, A.K.W., Qu, S., A study of formation of high order wheel polygonalization, Wear 424-425 (2019) 1-14.

144. Xu, J., Wang, K., Liang, X., Gao, Y., Liu, Z., Chen, R., Wang, P., Xu, F., Wei, K., Influence of visco-elastic mechanical properties of rail pads on wheel and corrugated rail rolling contact at high speeds, Tribology International, 151 (2020) 106523.

145. Xu, L., Gao, J., Zhai, W., On effects of rail fastener failure on vehicle/track interactions, Structural Engineering and Mechanics, 63 (2017) 659-667.

146. Yang, S.C., Kim, E., Effect on vehicle and track interaction of installation faults in the concrete bearing surface of a direct-fixation track, Journal of Sound and Vibration 331 (2012) 192-212.

147. Zhai, W., Wang, K., Horses, C., Fundamentals of vehicle-track coupled dynamics, Vehicle System Dynamics, 47(11), 2009, 1349–1376.

148. Zhang, X., Thompson, D.J., Squicciarini, G., Sound radiation from railway sleepers, Journal of Sound and Vibration 369 (2016) 178-194.

149. Zhang, X., Thompson, D. J., Li, Q., Kostovasilis, D., Toward, M., Squicciarini, G., Ryue, J. A model of a discretely supported railway track based on a 2.5D finite element approach Journal of Sound and Vibration 438 (2019) 153-174.

150. Zhang, P., Li, S., Núñez, A, Zili Li, Z., Multimodal dispersive waves in a free rail: Numerical modeling and experimental investigation, Mechanical Systems and Signal Processing 150 (2021) 107305.

151. Zhang, P., Li, S., Núñez, A., Li, Z., Vibration modes and wave propagation of the rail under fastening constraint, Mechanical Systems and Signal Processing 160 (2021) 107933.

152. Zhang, S., Cheng, G., Sheng, X., Thompson, D.J., Dynamic wheel-rail interaction at high speed based on time-domain moving Green's functions, Journal of Sound and Vibration 488 (2020) 115632.

153. Zhong, S., Xiong, J., Xiao, X., Wen, Z., Jin, X., Effect of the First Two Wheelset Bending Modes on Wheel–Rail Contact Behavior, Journal of Zhejiang University-Science A (Applied Physics & Engineering) 15(12), 2014, 984-1001.

154. Zhong, T., Chen, G., Sheng, X., Zhan, X., Zhou, L., Kai, J., Vibration and sound radiation of a rotating train wheel subject to a vertical harmonic wheel–rail force, Journal of Moderne Transportation 26 (2018) 81-95.

155. Zhu S. Y., Cai C.B., Luo, Z., Liao Z. Q., A frequency and amplitude dependent model of rail pads for the dynamic analysis of train-track interaction Science China Technological Sciences 58 (2015) 191-201.

156. Zhu, S., Cai, C., Spanos, P., A nonlinear and fractional derivative viscoelastic model for rail pads in the dynamic analysis of coupled vehicle–slab track systems, Journal of Sound and Vibration 335 (2015) 304-320.

157. Brüel & Kjær, Vibration test systems, www.bksv.com/vts.

158. C 116, Interaction between vehicles and track, RP 1, Power spectral density of track irregularities, Part 1: Definitions, conventions and available data, Utrecht, 1971.

159. EN ISO 3381: 2011, Railway applications – Acoustics – Measurement of Noise Inside Railbound Vehicles.

160. Instruction 314 on Norms and tolerances for the construction and maintenance of the track, Ministry of Transport and Telecommunications, 1989.

161. Instruction 341 for The composition, maintenance and supervision of the track without joists,

Societatea Națională a Căilor Ferate Române, 1997.

162. NI Compact DAQ – 9174, User manual, National Instruments, July 2011.

163. NL-602U ublox6 USB receptance, Manual operation.

164. Prospect: Vossloh Fastening Systems.

165. Technical specification of rubber rail plate for the fastening system type K, ST 02/2011, S.C. PROMIN PROD S.R.L.

166. SR EN 15663/2009 Railway applications – Definition of vehicle reference masses. 167. EN 13146-9 Railway applications - Track - Test methods for fastening systems - Part 9: Determination of stiffness

168. EN 13481-2 Railway applications - Track - Performance requirements for fastening systems - Part 2: Fastening systems for concrete sleepers.

169. EN 15610:2009, Railway Applications: Noise emission—Rail Roughness Measurement Related to Rolling Noise Generation, European Committee for Standardization, Brussels, Belgium, 2009.

170. ISO 10846-1 1997 Acoustics and vibration—Laboratory measurement of vibro-acoustic transfer properties of resilient elements—Part 1: principles and guidelines.

171. ISO 10846-2 1997 Acoustics and vibration—Laboratory measurement of vibro-acoustic transfer properties of resilient elements—Part 2: dynamic stiffness of elastic supports for translatory motion—direct method.

172. ISO/DIS 10846-3 1997 Acoustics and vibration—Laboratory measurement of vibroacoustic transfer properties of resilient elements—Part 3: dynamic stiffness of elastic supports for translatory motion—indirect method.

Published works

In this section are presented the titles of scientific papers published in the field of doctoral thesis during the doctoral training period.

I. PUBLISHED BOOKS

1. Cătălin Cruceanu, Camil Crăciun, Ioan Cristian Cruceanu, *Effects of braking characteristics on the longitudinal dynamics of short passenger trains,* Book Chapter in Rail TransportSystems Approach, Edited by: Sladkowski, A, Book Series: Studies in Systems Decision and Control, Volume 87, 2017, pp. 3-33, Publisher Springer International Publishing Ag, Gewerbestrasse 11, Cham, Ch-6330, Switzerland, ISBN 978-3-319-51502-1, 978-3-31951501-4, ISSN 2198-4182.

https://www.springerprofessional.de/en/effects-of-braking-characteristics-on-thelongitudinal-dynamics-/12130528

Accession number WOS: 000417897300002

II. ARTICLES / STUDIES IN EXTENSO PUBLISHED

Specialized magazines of international circulation, indexed in International Databases

1. Mădălina Dumitriu, **Ioan Cristian Cruceanu**, *Experimental analysis of vertical vibration of railway bogie,* currently being published in Communications - Scientific Letters of the

   University of Žilina, Issue 4/2021 (October 2021), ISSN 1335-4205. BDI indexed magazine: SCOPUS, Ebsco Host. http://komunikacie.uniza.sk/index.php/communications/about

   Journal metrics SCOPUS: Cite Score: 2.1/2020; SCImago Journal Rank (SJR): 0.288/2020; Source Normalized Impact per Paper (SNIP): 0.772/2020

2. Mădălina Dumitriu, **Ioan Cristian Cruceanu**, Dorina Fologea, *Experimental study of the bogie vertical vibration - correlation between bogie frame accelerations and wheelsets accelerations,* UPB Scientific Bulletin, Series D: Mechanical Engineering, Vol. 83, Issue 2, 2021, pp. 83-94, ISSN 1454-2358. https://www.scientificbulletin.upb.ro/SeriaD_-_Inginerie_Mecanica.php?page=revistaonline&a=1&cat=D

   BDI indexed journal: Ulrich's International Periodicals Directory, Scopus, Inspec, Metadex, Elsevier Sciences Bibliographic Databases, Engineering Village, Cambridge Scientific Abstracts, Compendex.

   Journal metrics SCOPUS: Cite Score: 0.6/2020; SCImago Journal Rank (SJR): 0.149/2020;

   Source Normalized Impact per Paper (SNIP): 0.316/2020

   SCOPUS indexed article

3. Mădălina Dumitriu, **Ioan Cristian Cruceanu**, *Effect of vertical track irregularities on the vibration of railway bogie*, UPB Scientific Bulletin, Series D: Mechanical Engineering, Vol. 81, Issue 1, 2019, pp. 67-78, ISSN 1454-2358. https://www.scientificbulletin.upb.ro/SeriaD_-_Inginerie_Mecanica.php?page=revistaonline&a=2&arh_an=2019&arh_ser=D&arh_nr=1

   BDI indexed journal: Ulrich's International Periodicals Directory, Scopus, Inspec, Metadex, Elsevier Sciences Bibliographic Databases, Engineering Village, Cambridge Scientific Abstracts, Compendex.

   Journal metrics SCOPUS: Cite Score: 0.6/2020; SCImago Journal Rank (SJR): 0.149/2020;

   Source Normalized Impact per Paper (SNIP): 0.316/2020 SCOPUS Indexed Article

   Article in which it is quoted:

   Wang Q., Liang S., *Dynamic analysis of tool changing system in power tool tower*, UPB

   Scientific Bulletin, Series D: Mechanical Engineering, Vol. 82, Issue 4, 2020, pp. 145-156 Indexed article: SCOPUS

4. Mădălina Dumitriu, **Ioan Cristian Cruceanu**, *On the rolling noise reduction by using the rail damper*, Journal of Engineering Science and Technology Review, Vol. 10, Issue 6, 2017, pp. 87-95, ISSN 1791-2377. DOI: 10.25103/jestr.106.12 http://www.jestr.org/index.php?option=com_content&view=article&id=55&Itemid=102

   BDI indexed magazine: SCOPUS, DOAJ, CERN, Google Scholar, EBSCO, ACS.

   Journal metrics SCOPUS: Cite Score: 1.2/2020; SCImago Journal Rank (SJR): 0.190/2020;

   Source Normalized Impact per Paper (SNIP): 0.491/2020

   Indexed article: SCOPUS, EBSCO

   Articles in which it is quoted:

1. T. Mazilu, D. Fologea, *Influence of the rail dampers on the frequency-domain response of the rail*, MATEC Web of Conferences - 22nd International Conference on Innovative Manufacturing Engineering and Energy - IManE&E 2018, Vol. 178, 2018, Article number 06021.

   DOI: 10.1051/matecconf/201817806021

   Indexed article: SCOPUS

2. T. Mazilu, D. Fologea, *Experimental study on the performance of a rail damper*, IOP Conference Series: Materials Science and Engineering, ModTech International Conference - Modern Technologies in Industrial Engineering, Vol. 400, 2018, Article number 062018.

   DOI: 10.1088/1757-899X/400/6/062018

   Indexed article: Web of Science, SCOPUS

   Accession number WOS: 000461147400160

3. T. Mazilu, D. Fologea, *Rail damper functionality-modelling and experimental determinations*, Materials Science Forum, Vol. 957, 2019, pp. 23-32. DOI: 10.4028/www.scientific.net/MSF.957.23 Indexed article: SCOPUS

4. T. Mazilu, I.R. Răcănel, G. Stoicescu, *Testing the functionality and performance of a rail damper*, Romanian Journal of Transport Infrastructure, Vol. 7, Issue 2, 2019, pp.

   31-39.

   DOI: 10.2478/rjti-2018-0010

   Indexed article: Web of Science

   Accession number WOS: 000460339200003

5. Haiping Liu, Dongmei Zhu, *Controlling the vibration and noise of a ballasted track using a dynamic vibration absorber with negative stiffness*, Proceedings of the Institution of Mechanical Engineers Part F Journal of Rail and Rapid Transit (FI 2,359/2020), 2019, Article Number UNSP 0954409719888084.

   DOI: 10.1177/0954409719888084

   Indexed article: Web of Science, SCOPUS

   Accession number WOS: 000499757000001

6. Sung D., Chang, S., Kim S., *Effect of additional anti-vibration sleeper track considering sleeper spacing and track support stiffness on reducing low-frequency vibrations*, Construction and Building Materials (FI 6.141/2020), Vol. 263, 2020, Article number 120140.

   DOI: 10.1016/j.conbuildmat.2020.120140

   Indexed article: Web of Science, SCOPUS

   Accession number WOS: 000582567100047

7. Kolesnikov V.I., Shapovalov V.V., Ozyabkin A.L., Shestakov M.M., Kornienko R.A., Pertseva T.D., Petrik A.M., *Selective suppression of amplitudes of frictional oscillations*, IOP Conference Series: Materials Science and Engineering, Vol. 900, Issue 1, 2020, Article number 012005.

   DOI: 10.1088/1757-899X/900/1/012005

   Indexed article: SCOPUS

Volumes of international scientific events, organized in the country and abroad, indexed in International Databases

1. Mădălina Dumitriu, Dorina Fologea, **Ioan Cristian Cruceanu**, *Effects analysis of vertical track irregularities on bogie vibration - method based on bogie modelling and wheelsets accelerations measurement*, 11th International Conference on Advanced Manufacturing

   Technologies (ICAMaT 2020), October 29 - 30, 2020, Bucharest, Romania, published in IOP Conf. Series: Materials Science and Engineering, Vol. 1018, 2021, Article number 012001, 9 pages.

   DOI: 10.1088/1757-899X/1018/1/012001

   https://iopscience.iop.org/article/10.1088/1757-899X/1018/1/012001

   Indexed article: SCOPUS

   Article in which it is quoted:

   Abid H.J., Hammood H., Swadi S.M., *Comparison between active suspension and regenerative suspension for full vehicle model*, Journal of Mechanical Engineering Research and Developments, Vol. 44, Issue 5, 2021, pp. 228 – 239.

   Indexed article: SCOPUS

2. **Ioan Cristian Cruceanu**, Ștefan Sorohan, *Determination of the harmonic response of a railway wheelset using the finite element analysis method*, The 13th International Conference Interdisciplinarity in Engineering, 3 – 4 October 2019, Tirgu Mures, Romania, published in Procedia Manufacturing, Vol. 46, 2020, pp. 173-179. DOI: 10.1016/j.promfg.2020.03.026

   https://www.sciencedirect.com/science/article/pii/S2351978920308970

   Indexed article: Web of Science, SCOPUS

   Category Web of Science: Engineering, Multidisciplinary; Engineering, Manufacturing Accession number WOS: 000582466200025

   Articles in which it is quoted:

1. Daniyan I., Mpofu K., Muvunzi R., Fameso F., Ramatsetse B., *Model design and finite element analysis of a traction link of a railcar*, Procedia CIRP, Vol. 100, 2021, pp. 37

   – 42.

   DOI: 10.1016/j.procir.2021.05.006

   Indexed article: SCOPUS

2. Liu Pengfei, Liu Hongjun, Wu Qing, *Estimation of wheelset natural vibration characteristics based on transfer matrix method with various elastic beam models*, Shock and Vibration (FI 1.543/2020), 2021, Article number 9973421.

   DOI: 10.1155/2021/9973421

   Indexed article: Web of Science, SCOPUS

   Accession number WOS: 000672270500005

3. Mădălina Dumitriu, Marius Alin Gheţi, **Ioan Cristian Cruceanu**, *Experimental analysis of the vertical vibration of the railway bogie during braking*, The 13th International

   Conference Interdisciplinarity in Engineering, 3 – 4 October 2019, Tirgu Mures, Romania, published in Procedia Manufacturing, Vol. 46, 2020, pp. 49-54. DOI: 10.1016/j.promfg.2020.03.009
   https://www.sciencedirect.com/science/article/pii/S2351978920308805

   Indexed article: Web of Science, SCOPUS

   Category Web of Science: Engineering, Multidisciplinary; Engineering, Manufacturing Accession number WOS: 000582466200008

   Article in which it is quoted:

   Szewerda K., Tokarczyk J., Wieczorek A., *Impact of increased travel speed of a transportation set on the dynamic parameters of a mine suspended monorail*, Energies (FI

   3,004/2020), Vol. 14, Issue 62, 2021, Article number 1528 DOI: 10.3390/en14061528

   Indexed article: Web of Science, SCOPUS

   Accession number WOS: 000634407900001

4. Traian Mazilu, **Ioan Cristian Cruceanu**, *Numerical study of the interaction between a moving oscillator and an infinite beam on elastic foundation with bilinear characteristic*, IOP Conf. Series: Materials Science and Engineering, The 8th International Conference on Advanced Concepts in Mechanical Engineering - ACME 2018, 13 – 16 June 2018, Vol. 444, 2018, Article number 042004. DOI: 10.1088/1757-899X/444/4/042004

   http://iopscience.iop.org/article/10.1088/1757-899X/444/4/042004

Indexed article: Web of Science, SCOPUS Category Web of Science: Mechanical Engineering

   Accesion number WOS: 000467443600040

5. Traian Mazilu, **Ioan Cristian Cruceanu**, *Dynamics of a beam on elastic foundation – impact of the bilinear characteristic of the foundation upon the propagation of the bending wave*, MATEC Web of Conferences - 22st Innovative Manufacturing Engineering & Energy International Conference – IManE&E 2018, Chisinau, Republic of Moldova, May 31 - June 2, 2018, Vol. 178, 2018, Article number 06008. DOI: 10.1051/matecconf/201817806008 https://www.matec-

   conferences.org/articles/matecconf/abs/2018/37/matecconf_imanee2018_06008/matecconf_imanee2018_06008.html

   Article indexed Web of Science, SCOPUS

   Category Web of Science: Engineering, Industrial; Materials Science, Multidisciplinary Accession number WOS: 000570197900085

   Article in which it is quoted:

Szewerda K., Tokarczyk J., Wieczorek A., *Propagation of periodic waves in beams on a bilinear foundation*, International Journal of Mechanical Sciences (FI 5.329/2020), 2021, Article number 106656.

DOI: 10.1016/j.ijmecsci.2021.106656

Indexed article: SCOPUS

6. Cătălin Cruceanu, Camil Crăciun, **Ioan Cristian Cruceanu**, *Effects of mechanical wheel slide protection devices action on railway vehicles braking process*, 19th International Conference on Innovative Manufacturing Engineering (IManE 2015), Iaşi, Romania, 21-22 May, 2015, published in Applied Mechanics and Materials, Vols. 809-810, Volume Innovative Manufacturing Engineering, 2015, pp. 1085-1090, Trans Tech Publications, Switzerland, ISSN 1662-7482, ISBN 978-3-03835-275-4. DOI:10.4028/www.scientific.net/AMM.809-810.1085 https://www.scientific.net/AMM.809-810.1085

Crossref, EBSCO, Google Scholar indexed article

Volumes of national scientific events

1. Mădălina Dumitriu, **Ioan Cristian Cruceanu**, *Analysis of the vertical vibrations of the Minden-Deutz bogie based on experimental data*, National Symposium of Railway Rolling Stock - XVII-th edition - Bucharest 2019, MatrixRom Publishing House, ISSN 1843-9888, pag. 98-107.

2. Mădălina Dumitriu, **Ioan Cristian Cruceanu**, *Methods and techniques for attenuating the noise emitted by the rail*, National Symposium of Railway Rolling Stock - XV-th edition – Bucharest 2017, MatrixRom Publishing House, pag. 161-185, ISSN 1843-9888.

3. Camil Crăciun, **Ioan Cristian Cruceanu**, Bogdan Voiculescu, *Unconventional railway vehicles monrail from Wupprtal*, National Symposium of Railway Rolling Stock - XV-th edition, Bucharest 2017, MatrixRom Publishing House, pp. 119-128, ISSN 1843-9888.

4. Traian Mazilu, **Ioan Cristian Cruceanu**, *Techniques for measuring noise in railway vehicles*, Railway Rolling Stock Symposium - XIV edition, Bucharest, 2016, Matrix Rom Publishing House, ISSN 1843-9888, pag. 116 - 125.